How to cite: *Angew. Chem. Int. Ed.* **2025**, *64*, e202421157
doi.org/10.1002/anie.202421157

Bioinorganic Chemistry Hot Paper

High-Valent Cobalt-Difluoride in Oxidative Fluorination of Saturated Hydrocarbons

*Agnideep Das, Brendan Twamley, Oscar R. Kelly, Chakadola Panda, Paul Richardson, and Aidan R. McDonald**

Abstract: The heme paradigm where Fe=O acts as the C–H oxidant and Fe–OH rebounds with the formed carbon-centered radical guides the design of the prototypical synthetic hydroxylation catalyst. We are exploring methods to evolve beyond the metal-oxo oxidant and hydroxide rebound, to incorporate a wider array of functional group. We have demonstrated the application of $Co^{II}(OTf)_2$ (10 mol% catalyst; OTf = trimfluoromethanesulfonate) in combination with polydentate N-donor ligands (e.g. BPMEN = N,N′-dimethyl-N,N′-bis(pyrid-2-ylmethyl)ethane-1,2-diamine) and Selectfluor in the oxidative fluorination of saturated hydrocarbons in high yields. The addition of CsF to the reaction mixture induced near-quantitative yields of fluorinated saturated hydrocarbons (>90% yield of fluorinated product). For 1-hydroxy, 1-acetyl, 1-carboxy-, and 1-acetamido-adamantane, we demonstrated selective fluorination at the 3-position. We propose two mechanisms for the Co^{II}-catalyzed reaction: *either* (i) an N-radical, derived from Selectfluor, acted as the C–H oxidant followed by radical rebound with Co^{III}–F; *or* (ii) a Co^{IV}–$(F)_2$ species was the C–H oxidant followed by radical rebound with Co^{III}–F. Our combined spectroscopic, kinetic, and chemical trapping evidence suggested that an N-radical was not the active oxidant. We concluded that a Co^{IV}–$(F)_2$ species was the likely active oxidant and Co^{III}–F was the likely F-atom donor to a carbon centered radical producing a C–F bond.

[*] A. Das, B. Twamley, O. R. Kelly, C. Panda, A. R. McDonald
School of Chemistry, Trinity College Dublin, The University of Dublin, College Green, Dublin 2, Irelandhttps://chemistry.tcd.ie/staff/people/mcdonald
E-mail: aidan.mcdonald@tcd.ie

C. Panda
Department of Chemistry, Science Faculty, University of Allahabad, Prayagraj, Uttar Pradesh 211002, India

P. Richardson
Medicine Design, Pfizer La Jolla, 10770 Science Center Drive, La Jolla, California, 92121, USA

Introduction

The oxidative activation of saturated hydrocarbons remains challenging primarily due to the inertness of the C–C and C–H bonds found in these abundant substrates.[1] Nature has evolved to functionalize saturated hydrocarbons via a two-step process where the C–H bond is first broken through high-valent oxidant mediated proton coupled electron transfer (PCET) oxidation followed by introduction of functional groups through metal-mediated radical rebound (RR).[2] A prototypical example of this is the nonheme iron halogenases where dioxygen activation at Fe^{II} yields a Cl–Fe^{IV}=O oxidant that cleaves the C–H bond through PCET followed by RR between the formed C-centered radical and a Cl–Fe^{III}–OH entity to yield chlorinated hydrocarbon (Figure 1).[3] This process relies on the enzyme active site ensuring selective RR of the Fe-bound Cl ligand rather than the hydroxide. The natural function of nonheme iron halogenases are limited to chlorination and bromination, however, engineered nonheme iron enzymes have recently been demonstrated to be capable of radical fluorination of saturated hydrocarbons.[4] The engineered systems rely on N-fluoride substrates that are primed for radical fluorination, but do not employ an Fe^{IV} oxidant. Nature's process for saturated hydrocarbon functionalization is highly effective, as long as sufficiently potent high-valent PCET oxidants can be generated, alongside effective means for RR.

Synthetic complexes that facilitate the oxidative halogenation of saturated hydrocarbons have displayed promise, being capable of mimicking nonheme iron halogenase function, if not always selectivity.[5] Of particular note are the synthetic X–Fe^{IV}=O (X = Cl, Br) that acted as both structural and functional mimics of the nonheme iron halogenases.[5b,6] In some cases these complexes were capable of incorporating halogens into saturated hydrocarbons, although they have suffered from competitive hydroxide rebound. X–Fe^{III}–OH products were primed for hydroxide rebound without the protein structure to control rebound as observed in the halogenases. Interestingly, computational analyses have predicted that hydroxide rebound is thermodynamically preferred over halide rebound.[7]

Fluorination of small-molecules is a widely employed tactic to enhance the bioavailability and stability of medicines.[8] Furthermore, the rapid incorporation of F-atoms into small-molecules is of particular interest to those developing ^{18}F radio-tracers.[9] Traditional methods for this rely on elemental F_2, XeF_2, or HF, a group of highly reactive

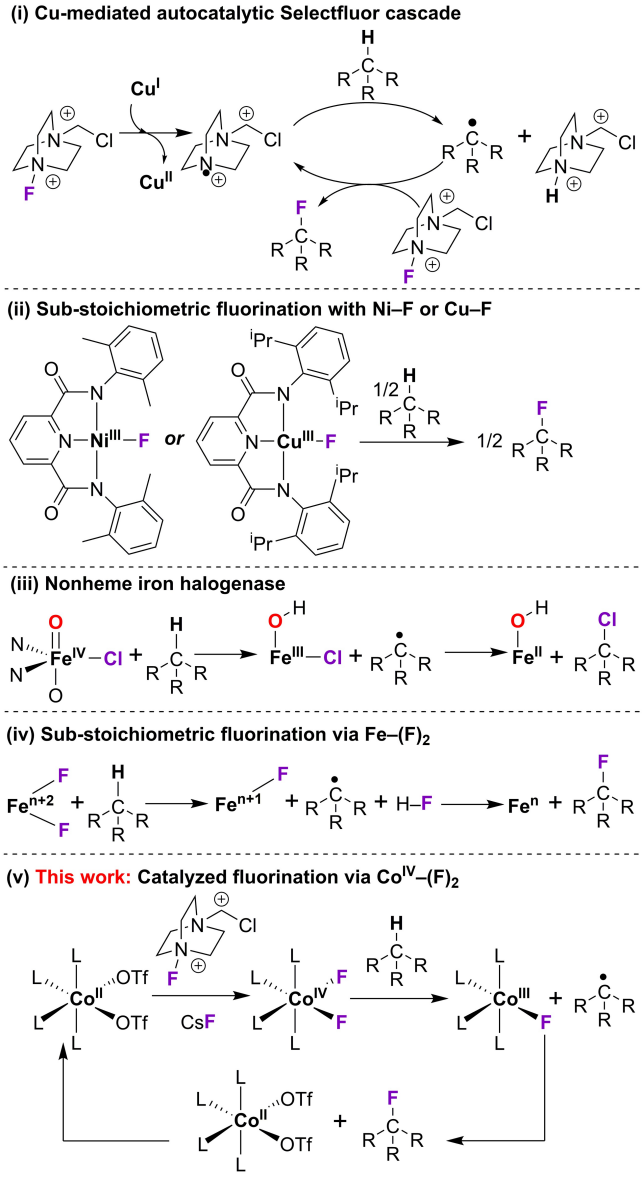

Figure 1. Metal-mediated oxidative fluorination of saturated hydrocarbons and nonheme iron catalyzed chlorination.

indiscriminate oxidants with significant toxicity risks.[10] In these cases, F• was proposed to both perform C–H activation and F-atom donation. Generally these reagents display poor selectivity and high levels of substrate degradation due to the high potential of the oxidant ($F^{\bullet} \rightarrow F^{-}$; $E^{0} = 2.87$ V).[11] Molecular electrophilic and nucleophilic fluorinating reagents have been developed that mitigate some of the toxicity risks, although they are often only effective on activated substrates.[8b,10a,12] Metal-mediated oxidative radical fluorination represents an opportunity to perform hydrocarbon fluorination on a scale and at a cost commensurate with the abundance of these substrates, as long as we can develop simple catalysts that allow control over both the oxidant *and* the F-atom donor (which may be the same entity or different species). We envisage mimicking heme and nonheme iron methods for hydrocarbon hydroxylation,[13] replacing the heme paradigm of C–H activation by Fe=O followed by radical rebound by Fe–OH, with high-valent metal-difluorides (M–$(F)_2$) that facilitate both C–H activation and fluorine atom transfer.

Groves and co-workers developed a process where the oxidant and F-atom donation were performed by separated entities—a $Mn^{V}=O$ was the postulated PCET C–H oxidant, followed by RR between the formed C-carbon-centered radical and a Mn^{IV}–F.[5a,6g,14] Saturated hydrocarbon (C-(*sp3*)–H) fluorination was achieved in reasonably good yields (up to 57 %), however, this process likely suffered from competitive hydroxide rebound. Lectka and co-workers have shown that the combination of Selectfluor (SF) and Cu^{I} in the presence of diamine ligands allowed for fluorination of C(*sp3*)–H bonds.[15] It was determined that Cu^{I} facilitated an initial N–F bond scission in SF yielding an N-radical species called $TEDA^{\bullet+}$ (N-(chloromethyl)triethylenediaminyl radical) and Cu^{II}–F (Figure 1). $TEDA^{\bullet+}$ was determined to be the active oxidant yielding substrate carbon radicals that reacted with another molecule of SF to yield fluorinated product and $TEDA^{\bullet+}$. After the initial involvement of Cu^{I} in SF activation, the metal played no further role. Many others have demonstrated that SF acted as a remarkably useful platform for hydrocarbon fluorination following the same mechanism.[12d,16] In most of these examples, modest-to-good yields of the fluorinated products were achieved (generally < 75 %).

We have explored high-valent metal-halide complexes for their capabilities as strong oxidants in C–H activation *and* in hydrocarbon halogenation (Figure 1).[17] We postulated that high-valent metal-halides can be potent oxidants because of the magnitude of the H–X (X = halide) bond that acts as the thermodynamic driver for PCET by metal-halides. Indeed, we demonstrated that Ni^{III}–F and Fe^{III}–F oxidants were some of the most reactive high-valent oxidants reported to date. The Ni^{III}–F was also capable of the fluorination of ethylbenzene in 11 % yield.[17b] At the same time, Zhang, Stieber, and co-workers demonstrated that the corresponding Cu^{III}–F complex was capable of sub-stoichiometric fluorination of hydrocarbons in up to 50 % yield.[18] Co–F compounds have been identified as useful fluorinating reagents capable of both electrophilic and nucleophilic fluorinations,[19] as well as F-atom radical transfer fluorination of olefins or other highly activated substrates.[20] In anticipation that a M–$(F)_2$ entity might act to both abstract an H-atom with one F-ligand and donate an F-atom with the other, we showed that the combination of an Fe^{II} complex and difluoro(phenyl)-λ^3-iodane ($PhIF_2$) facilitated sub-stoichiometric C–H bond fluorination in modest yields (2–50 % yield).[17f] A kinetic analysis suggested that an Fe^{IV}–$(F)_2$ entity was the likely PCET C–H oxidant, followed by RR with an Fe^{III}–F to yield fluorinated product. Our explorations to date have thus shown high-valent metal-fluorides to be exceptional oxidants capable of breaking the strongest of C–H bonds under *sub-stoichiometric* reactivity conditions. Herein, we describe our efforts towards developing catalytic fluorination of saturated hydrocarbons via a high-valent metal-difluoride adduct that acts both to activate the C–H bond via PCET and to donate an F-atom by RR.

Results and Discussion

Catalysis Studies

Screening of ligand and metal salts for C–H fluorination: We targeted the oxidative fluorination of simple (inert) saturated hydrocarbons (Scheme 1). In our initial efforts, we were hindered by the poor solubility of certain saturated hydrocarbons, and thus settled on 1-adamantanol as a suitable model substrate because it contains strong C–H bonds and allows for an assessment of selectivity (tertiary (bond dissociation free energy (BDFE) ≈ 97 kcal/mol) versus secondary (~100 kcal/mol) C–H bonds), while also being soluble in CH_3CN.[21] Under anaerobic conditions, 1-adamantanol, a metal salt or complex, and (where employed) a ligand were dissolved in anhydrous CH_3CN followed by addition of Selectfluor (SF, 1-(chloromethyl)-4-fluoro-1,4-diazabicyclo[2.2.2]octane-1,4-diium di-tetrafluoroborate, see Supporting Information file for details). Reaction progress and yields were monitored using ^{19}F nuclear magnetic resonance (NMR) spectroscopy allowing us to follow the consumption of SF and the formation/yield of any fluorinated hydrocarbon products. When formed, 3-fluoro-1-adamantanol (3FA) produced a ^{19}F NMR signal at $\delta = -133.4$ ppm (Figure S1). Two signals at $\delta = +46$ and -151 ppm, were assigned to the SF N–*F* group and the $^{-}BF_4$ anion, respectively. The yield of 3FA *and* the degree of consumption of SF could be assessed through integration of the signals associated with each entity with respect to the integral for the $^{-}BF_4$ signal (which was not consumed during the reaction).[22]

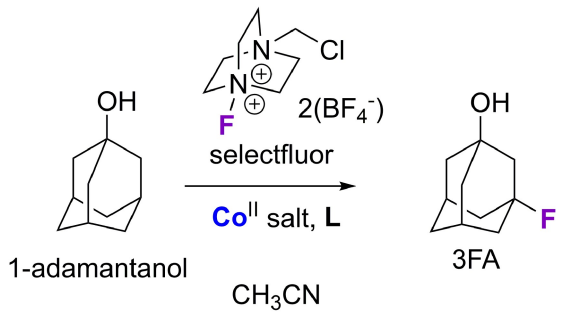

Scheme 1. Screening of Co^{II}-catalyzed oxidative fluorination of 1-adamantanol using Selectfluor (SF). L = ligand (see Figure 2 for examples), 3FA = 3-fluoro-adamantan-1-ol.

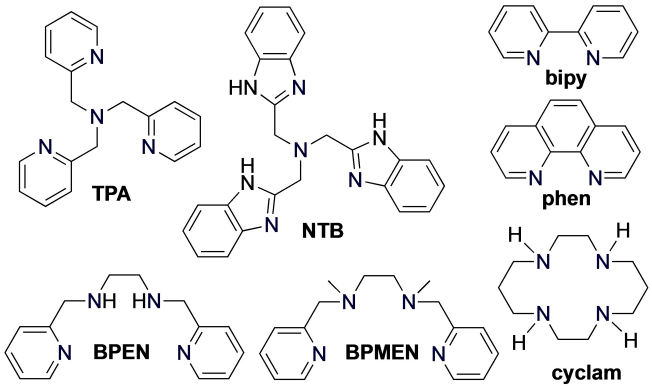

Figure 2. Ligands screened in the Co-catalyzed oxidative fluorination of saturated hydrocarbons.

Our initial screen indicated that Co^{II} salts combined with a simple polydentate N-donor (TPA, tris(2-pydridylmethyl)amine, Figure 2) were promising candidates for hydrocarbon fluorination (Table 1). In the absence of TPA, no fluorinated product nor significant consumption of SF was observed. Likewise, in the absence of Co^{II}, no fluorination products were identified although near-complete (96 %) depletion of SF was observed. Once Co^{II} salts were combined with TPA, we observed a good yield of 3FA (45 %) alongside near complete consumption of SF (83 %) at 20 °C. Heating to 50 °C provided a slight enhancement in yield (48 %), alongside complete SF consumption. At higher temperature (75 °C) we observed a drop in the quantity of 3FA and ^{19}F NMR resonances at $\delta = -138.7$–174.1, and -190.0 ppm that could be assigned to the 3,5-difluoroadamantan-1-ol (35DFA),[16b] 2-fluoroadamantanol (2FA),[23] and 4-fluoroadamantanol (4FA[23]) products, respectively (Figure S2). The 35DFA is a product of over-fluorination while the 2FA and 4FA are assumed to form in negligible quantities at low temperature, only appearing at measurable levels at high temperatures. As with higher temperatures, longer reaction time (18 h) also produced 35DFA, 2FA, and 4FA. Interestingly, the combination of an Fe^{II} salt and TPA gave a poor yield of 3FA (< 2 %), despite significant SF depletion. Finally, when we employed $[Co^{II}(NCCH_3)(TPA)](OTf)_2$, rather than simply combining the metal salt and ligand in the reaction vessel, we observed no difference in the yield of 3FA (see Supporting Information for details of $[Co^{II}(NCCH_3)(TPA)](OTf)_2$ preparation, Figures S3–S9).

We expanded our ligand screening in order to identify the ideal supporting ligand for hydrocarbon fluorination (Figure 2, Table 2). The NTB ligand (a tripodal tetradentate benzimidazole analogue of TPA) combined with Co^{II} did not produce any 3FA, nor did it induce SF activation. Simple

Table 1: Initial screening of catalysts and conditions.

Metal salt/complex[a]	Ligand	t (h)	T (°C)	SF consumed (%)	3FA yield (%)
–	–	2	20	5	0
–	–	2	50	5	0
$Co(OTf)_2$	–	2	50	7.5	0
–	TPA	2	50	96	0
$Co(OTf)_2$	TPA	2	20	83	45
$Co(OTf)_2$	TPA	2	50	100	**48**
$Co(OTf)_2$	TPA	2	75	100	28[b]
$Co(OTf)_2$	TPA	18	50	100	17[b]
$Fe(OTf)_2$	TPA	2	50	70	< 2
$[Co^{II}(TPA)](OTf)_2$	–	2	50	82	49
$[Co^{II}(TPA)](OCl_4)_2$	–	2	50	100	43

[a] 50 mol% catalyst loading, thus 2 equiv. SF was used. [b] 35DFA and 2FA/4FA identified in reaction mixture.

Table 2: Ligand and metal salt screening.[a]

Metal salt	Ligand	SF consumed (%)	3FA yield (%)
$Co(OTf)_2$	TPA	100	48
$Co(OTf)_2$	NTB	5	0
$Co(OTf)_2$	bpy	100	40
$Co(OTf)_2$	1,10-phen	65	20
$Co(OTf)_2$	cyclam	100	31
$Co(OTf)_2$	BPEN	97	46
$Co(OTf)_2$	BPMEN	97	**56**
$Co(ClO_4)_2 \cdot 6H_2O$	BPMEN	85	50
$CoCl_2$	BPMEN	63	10
$[Co^{III}(Cl)(TPP)]$[b]	–	50	0
$[Co^{II}(TMP)]$[c]	–	50	0
$Fe(OTf)_2$	TPA	70	<2
$Fe(OTf)_2$	NTB	80	19
$Fe(OTf)_2$	BPY	95	0
$Fe(OTf)_2$	1,10-phen	55	0
$Fe(OTf)_2$	cyclam	100	2
$Fe(OTf)_2$	BPEN	93	3
$Fe(OTf)_2$	BPMEN	56	5
[Fe(Cl)(TPP)][b]	–	50	0
$Ni(OTf)_2$	BPMEN	100	0
$Cu(OTf)_2$	BPMEN	85	15
Cu(OTf)	BPMEN	100	8
[Cu(BEN)(I)][d]		100	11

[a] Conditions: t = 2 h; T = 50 °C; SF equiv. = 2 (50 mol% catalyst); solvent = CH_3CN. [b] TPP = tetraphenylporphyrin. [c] TMP = tetramesitylporphyrin. [d] BEN = *N*,*N*′-bis(benzylidene)ethane-1,2-diamine (10 mol% catalyst).

bidentate ligands 2,2-bipyridine (bpy) and 1,10-phenanthroline (phen) both produced reasonable yields of 3FA when combined with $Co^{II}(OTf)_2$ (40 % and 20 %, respectively). The macrocylic tetra-secondary amine donor, cyclam, produced a 31 % yield of 3FA. The linear tetra-dentate polypyridine ligands BPEN and BPMEN, showed 46 % and 56 % yields of 3FA in combination with $Co^{II}(OTf)_2$. Finally, when an anionic N-donor supporting ligand was employed (in this case tetraphenylporphyrin or tetramesitylporphyrin) we observed no fluorinated product and limited SF consumption, whether it was a Co^{II} *or* Co^{III} catalyst. We concluded that all pyridine- and alkylamine-containing ligands were effective in combination with Co^{II}, whereas the benzimidazole-containing NTB and porphyrins were not. Cyclam coordinates to metals in a *meridional* fashion inducing ancillary ligand binding in positions *trans* to one-another. For bpy and phen, the location of ancillary binding sites could either be *cis* or *trans* depending on the number of ligands coordinated and the relative positioning. We tentatively conclude that cyclam/bpy/phen don't provide the optimal coordination environment for effective fluorination (these ligands displayed 3FA yields of $\leq$40 %). In contrast, TPA, BPEN, and BPMEN generally induce *cis*-α or *cis*-β ligation at a metal,[24] yielding ancillary labile sites *cis* to one-another—we surmise this represents the optimal geometric conditions for hydrocarbon fluorination (3FA yields $>$40 %).

Given our observations that BPMEN produced the highest yields of hydrocarbon fluorination, we pursued the application of Co^{II}/BPMEN-catalyzed fluorination in greater detail. We explored a number of alternative metal salt/anion combinations and found that Co^{II} sources with labile counterions (^{-}OTf, $^{-}ClO_4$) displayed the highest yields of fluorination ($>$50 %). In contrast, the less-labile ^{-}Cl ligand in $CoCl_2$ produced 3FA in just 10 % yield, indicating ease of ancillary ligand displacement at Co^{II} was important. This mirrors the result obtained for $[Co^{II}(TMP)]$ where the anionic supporting ligand appeared to inhibit fluorination.

Previous success has been achieved with Cu^{I}/SF and Fe^{II}/SF systems for hydrocarbon fluorination, we therefore felt it prudent to screen other metals (Table 2).[15a,b,e] A combination of $Fe^{II}(OTf)_2$, NTB, and SF produced 3FA in 19 % yield, although not matching the levels observed with Co^{II} catalysts. Somewhat surprisingly, this was the only Fe^{II}/ligand combination that produced noteworthy yields of 3FA. For all other Fe^{II}/L combinations we observed yields of 3FA $\leq$ 5 %. High degrees of SF consumption were observed in all instances (50–100 % SF depletion). This suggests that Fe^{II} salts were capable of inducing N–F bond activation in SF, but the resulting products either could not break strong C–H bonds or were ineffective fluorinating agents. In fact, almost all Fe^{II}, Ni^{II}, Cu^{II}, and Cu^{I} salts that we tested produced low yields of 3FA despite facilitating the near-complete decay of SF. Of particular note are the Cu^{I} and Cu^{II} salts that demonstrated 8 % and 15 % yields of 3FA, in marked contrast to previous examples where Cu-catalyzed SF-mediated fluorination was achieved in $>$50 % yields under different, somewhat more convoluted conditions.[15a,e] Indeed we tested the [Cu(BEN)(I)] catalysts developed by Lectka, under the current conditions, showing complete SF consumption, but just 11 % yield of 3FA. We concluded that Co^{II} appears to represent a sweet-spot for saturated hydrocarbon fluorination.

In an effort to identify the active catalyst and probe the catalytic mechanism, we pursued the synthesis of $[Co^{II}(BPMEN)]^{2+}$ (see Supporting Information file for details, Figures S10–S16). Briefly, a CH_3CN solution of $Co^{II}(OTf)_2$ was mixed with BPMEN at room temperature for 16 h, producing an orange solution. Recrystallization from CH_3CN/Et_2O yielded pale pink crystals suitable for X-ray diffraction measurements. These measurements confirmed the structure as $[Co^{II}(BPMEN)(OTf)_2]$ (defined as **1**, Figure 3), with the Co^{II} ion in a *pseudo*-octahedral environment ligated by the four N-donors of the BPMEN ligand and two O-donors of monodentate ^{-}OTf ligands. The ^{-}OTf were ligated *cis* to one another, with the BPMEN ligand demonstrating a *cis*-α geometry,[24] where the two pyridine donors were *trans* to each other and *cis* to the alkylamine and ^{-}OTf donors. BPMEN-supported first row transition metal complexes (e.g. Mn,[25] Fe,[25a,26] Co,[27] Ni,[28] Cu,[28b,29] Zn[30]) have been synthesized and employed in a variety of catalysis applications. Yang and co-workers previously reported the preparation of $[Co^{II}(BPMEN)(NCCH_3)_2](BF_4)_2$ which displayed two Co-bound CH_3CN molecules, displaying comparable structural properties.[27] **1** was thus similar to

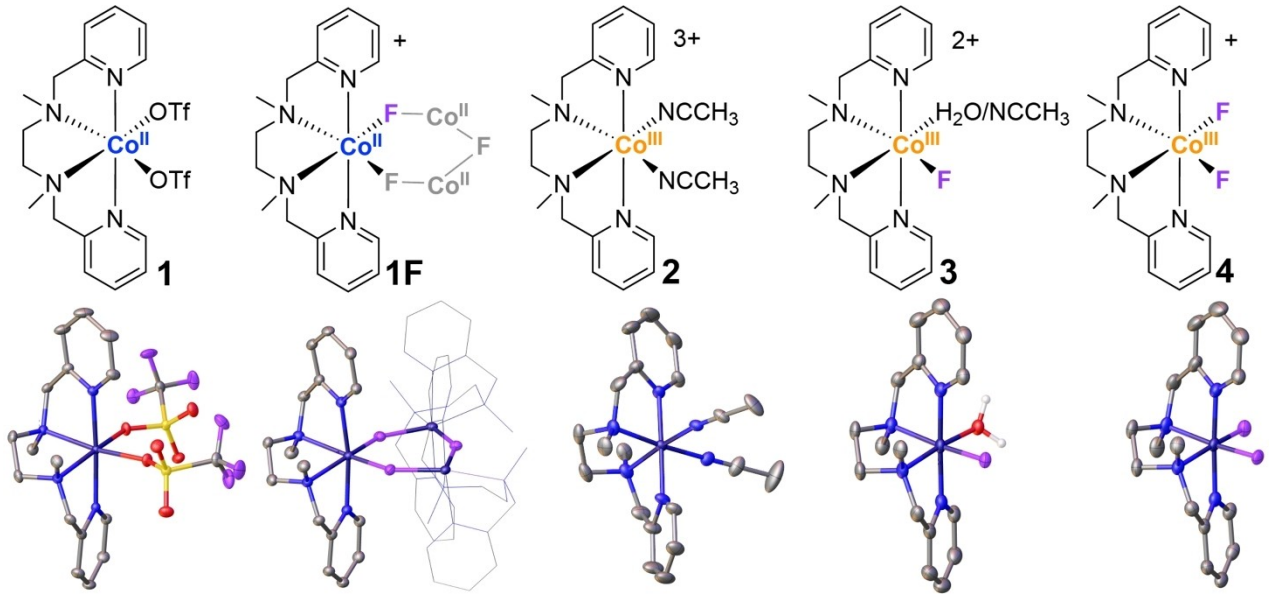

Figure 3. Molecular drawings (top) and ORTEPs of **1**, **1F**, **2**–**4** (bottom) complexes and ions. H-atoms (except for coordinated H_2O in **3**), solvent molecules, additional BPMEN ligands in **1F**, and non-binding counter anions were omitted for clarity.

other linear tetradentate transition metal complexes, critically displaying *cis*-labile binding sites on the Co center.

^{1}H NMR of **1** in CD_3CN showed broad and significantly shifted signals consistent with the presence of a paramagnetic metal ion (Figure S10). Seven signals were observed ranging from $\delta = +220$ ppm to $+20$ ppm, suggesting the BPMEN ligand was in a symmetric environment in **1** in solution (consistent with the solid-state X-ray crystal structure data). An Evan's method calculation of the effective magnetic moment suggested $\mu_B = 4.24$ Bohr magneton (Figure S11), which corresponds to an $S = 3/2$ d^7 Co^{II} ion in a *pseudo*-octahedral environment. Co^{II} complexes with polyamine ligands or macrocyclic ligands were commonly found in such a high-spin d^7 state.[31] In contrast, stronger field porphyrin supported Co^{II} complexes were low-spin ($S = \frac{1}{2}$).[32] ^{19}F NMR analysis of **1** showed a signal at $\delta = -79.1$ ppm consistent with free $^-$OTf (Figure S12), suggesting that the $^-$OTf were labile in solution.

Electron paramagnetic resonance (EPR) spectroscopy of **1** in the solid state displayed a very broad signal centered at $g = 3.8$ at 77 K (Figure S13), while ^{59}Co hyperfine was not observed. Similarly broad EPR spectra centered at $g \sim 4$ were observed in Co^{II}-salen (salen = (R,R')-N,N'-bis(3,5-di-tert-butylsalicylidene)-1,2-cyclohexane-diamino),[33] Co^{II}-oxide,[34] Co^{II}-phosphine,[35] and Co^{II}-cyanide complexes.[36] Electrospray ionization mass-spectrometry (ESI-MS) analysis of **1** showed three signals at m/z = 164.5686, 364.0888, and 478.0720 which can be attributed to the cations $[Co^{II}(BPMEN)]^{2+}$, $[[Co^{II}(BPMEN)] + Cl]^+$, and $[[Co^{II}(BPMEN)] + OTf]^+$, respectively (Figure S14). In summary, **1** was a *pseudo*-octahedral complex with a tetradentate ligand coordinated in a *cis*-α fashion, leaving labile ligands at sites *cis* with respect to each other at Co^{II}. When **1** was applied as a catalyst in 1-admantanol fluorination, the yield of 3FA was the same as when BPMEN and $Co^{II}(OTf)_2$ were separately combined in the reaction mixture (Table 3), demonstrating that **1** was the active catalyst or a precursor to the active catalyst.

Using $Co^{II}(OTf)_2$/BPMEN, we endeavored to optimize the yield of fluorinated products through screening of the reaction time, temperature, and catalyst loading (Table 3). At room temperature (20 °C) a maximum yield of 57 % was obtained after an 18 h reaction, after 2 h the yield was 42 %. Heating to 50 °C allowed us to achieve 56 % yield of 3FA after just 2 h, whereas heating at 50 °C for an extended period (18 h) resulted in a lower yield of 3FA (27 %). Heating at 75 °C for 2 h also decreased the yield of 3FA (27 %). As observed for the Co^{II}/TPA combination, a longer reaction time and/or heating to 75 °C resulted in the formation of 35DFA, 2FA, and 4FA for Co^{II}/BPMEN. All reactions to this point were performed under 50 % catalyst loading (thus two equiv. of SF per Co). In moving to 20 mol% and then 10 mol% Co, we observed the same yields of 3FA (~55 %) when reactions were performed at 50 °C, whereas at 20 °C lower yields of 3FA were obtained (29 %). At catalyst loadings lower than 10 mol% the yield of 3FA dropped below 50 % (7.5 mol% Co^{II}).

A significant improvement in the yield of 3FA was obtained upon addition of CsF (10 equiv.) resulting in near-quantitative yields of 3FA (91 %, Figure S17). In contrast, other inorganic fluoride sources had little impact on the yield of 3FA (~50 %). All inorganic fluoride sources displayed poor solubility under the reaction conditions. Addition of a soluble 'organic' fluoride source (tetrabutylammonium fluoride, TBAF) resulted in markedly lower yield of 3FA (13 %). We attribute this to the presence of additional H_2O of crystallization that was present in the TBAF. We have observed previously that H_2O can inhibit PCET by high-valent metal-fluoride complexes.[17b] Importantly, the highest yields of 3FA were obtained alongside

Table 3: Optimization of Co^{II}/BPMEN fluorination catalysis conditions.

Catalyst	t (h)	T (°C)	additive	Co loading (mol%)	SF equivalents	SF consumed (%)	3FA yield (%)
$Co(OTf)_2$/BPMEN	2	20		50	2	78	42
$Co(OTf)_2$/BPMEN	18	20		50	2	92	57
$Co(OTf)_2$/BPMEN	2	50		50	2	97	56
$Co(OTf)_2$/BPMEN	18	50		50	2	100	27[a]
$Co(OTf)_2$/BPMEN	2	50		20	5	95	54
$Co(OTf)_2$/BPMEN	2	20		10	10	49	29
$Co(OTf)_2$/BPMEN	2	50		10	10	93	56
$Co(OTf)_2$/BPMEN	2	75		10	10	94	27[a]
$Co(OTf)_2$/BPMEN	2	50		7.5	15	84	44
BPMEN	2	50		10	10	72	0
1	2	50		10	10	93	56
1	2	50	KF	10	10	73	49
1	2	50	CsF	10	10	100	***91***
1	2	50	AgF	10	10	81	35
1	2	50	CaF_2	10	10	90	51
1	2	50	ZnF_2	10	10	87	53
1	2	50	$TBAF.H_2O$	10	10	83	13
1F	2	50			10	63	46
1F	2	50	CsF	10	10	70	66
2	2	50		10	10	9	3
4	2	50		10	10	9	0

[a] over-fluorination product 35DFA, as well as 2FA and 4FA identified in reaction mixture.

the highest levels of SF consumption. SF consumption levels were consistently above 90% in the presence of Co^{II} once the reaction mixture was heated to 50°C. Overall, our optimization studies indicated that 50°C was the optimal reaction temperature, with 10 mol% catalyst loading, and the addition of an external inorganic fluoride source (CsF) allowing us to reach near-quantitative yields of 3FA.

In order to assess the role of CsF, we probed the addition of CsF to **1** in CD_3CN: we observed shifts in ^1H NMR resonances assigned to **1** indicating the formation of a new Co^{II} complex, defined as **1F** (Figure S18). Based on the similarities in the NMR spectra, we surmised the replacement of the coordinated ^-OTf anion with ^-F, while a symmetric environment was maintained. The ^{19}F NMR of **1F** displayed a signal for free ^-OTf, but no resonance that could be assigned to the metal bound Co–F signal (Figure S19). Layering a CH_3CN solution of **1F** with Et_2O yielded pale pink crystals suitable for X-ray diffraction, which showed **1F** to be a Co^{II}-μ-F trimer, where Co^{II} and F occupied six alternate corners of a hexagon (Figure 3). Three ^-OTf were found in the crystal lattice, confirming the Co^{II} oxidation state was maintained. The BPMEN ligand remained bound in a cis-α fashion at Co, while the $Co–N_{py}$ bond lengths were comparable to those in **1** (2.130 Å in **1F**, 2.126 Å in **1**). The $Co–N_{am}$ bonds were slightly elongated (2.208 Å in **1F**, 2.164 Å in **1**). The Co–F = 2.036 Å was longer than in the Co^{III} complexes **3** and **4** (1.868 and 1.850 Å respectively, see below) and the previously reported $[Co^{III}(F)_3(Me_3TACN)]$ (1.857–1.871 Å, Me_3TACN = 1,4,7-trimethyl-1,4,7-triazacyclononane), consistent with the lower oxidation state.[37] ESI-MS of **1F** showed peaks at m/z = 348.1218 and 845.1820 that can be attributed to the cations $[Co^{II}+BPMEN+F]^+$ and $[[Co^{II}+BPMEN+F]_2+OTf]^+$ respectively (Figure S20). FT-IR of **1F** displayed a signal at $\nu_{Co–F} = 571\ cm^{-1}$ which was comparable to other $\nu_{Co–F}$ (described below, Figure S21). Importantly, when **1F** was used as a catalyst (10 mol% Co^{II}, 3.3 mol% **1F**), a 46% yield of 3FA was obtained (66% with CsF).

After optimizing the reaction conditions, a series of saturated hydrocarbon substrates were screened (Scheme 2), and the crude reaction mixtures were analyzed by ^{19}F NMR (Table S1, Figures S22–S36). The poorly soluble adamantane was converted to 1-fluoroadamantane in reasonably good yield (38%). An enhanced yield in the presence of CsF was observed (63%). 1-adamantane-carboxylic acid and 1-acetyladamantane were converted into the corresponding 3-fluoro-substituted products in yields comparable to that obtained for 1-adamantanol (55% and 56%, respectively), also showing an improved yield when the reaction was carried in the presence of CsF (78% and 66%, respectively). 1-aminoadamantane did not produce any fluorinated product, however, once the amine was protected as an amide, a reasonable yield (54%) of 3-fluorinated product was obtained. For all of the adamantane-derived substrates we observed high degrees of selectivity for the tertiary C–H bond at the 3-position, which is the slightly weaker bond with respect to the secondary 2- and 4-C–H groups. We surmise that the oxidant was selectively activating this weaker bond *or* that the ligand framework was inducing selective C–H activation through a steric effect. Moving

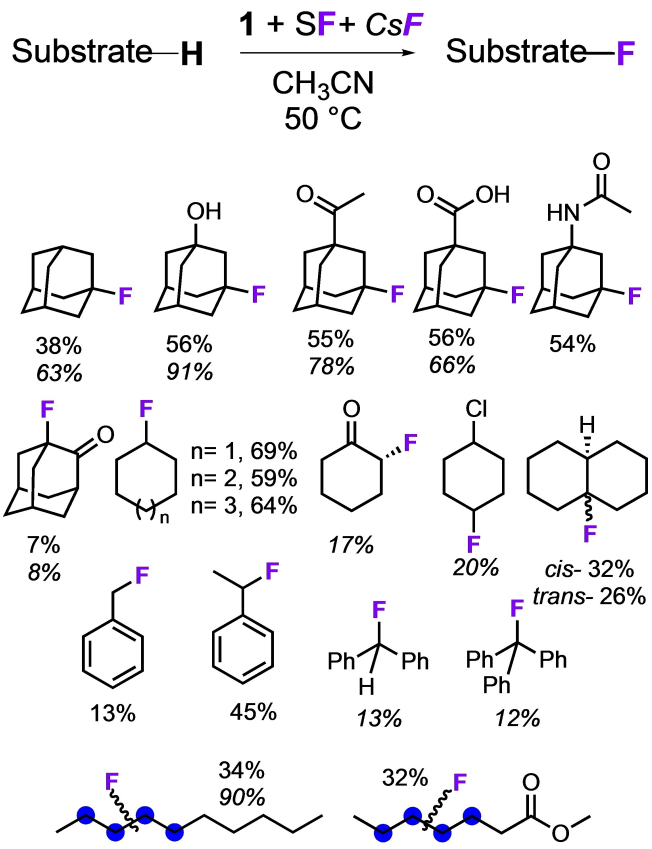

Scheme 2. Substrate screening studies. Conditions: **1** (10 mol%), 50 °C, 2 h. Yield determined using ^{19}F NMR. *Italicized* yields were determined when CsF (10 equiv.) added. References for ^{19}F signals:[15a,e,16b,c,17f,23,38]

beyond 1-adamantanol and analogues, cyclohexane (69 %), cycloheptane (59 %), cyclooctane (64 %), decalin (58 %), n-decane (34 %), and methylheptanoate (32 %) all displayed reasonable yields of the corresponding mono-fluorinated products. Lower degrees of selectivity were observed for *trans*-decalin (*cis*- and *trans*-fluoro-decalin obtained in comparable yields) and n-decane (signals for fluorination at all C–H positions observed). *n*-decane also displayed increased fluorination yield when CsF was used as an additive (90 %). Finally, 1-chlorocyclohexane was converted to *trans*-1-chloro-4-fluorocyclohexane in 20 % yield demonstrating that there is a degree of compatibility with other halo-alkanes.

Some substrates provided lower than anticipated yields of fluorination: 2-adamantanone displayed low yields of fluorination in the presence and absence of CsF (7 % and 14 %, respectively). Likewise, cyclohexanone yielded 2-fluoro-cyclohexanone in 17 % yield. Toluene and ethylbenzene displayed low yields of the fluorinated products fluoromethylbenzene and 1-fluoro-1-phenylethane, respectively. Furthermore, diphenylmethane and triphenyl methane also displayed relatively low yields of fluorination (when compared to adamantane-derived substrates). With these α-keto- and α-aryl-substrates we also observed a low degree of SF consumption, indicating the Co^{II} catalyst had been deactivated during the reaction. We ascribe this to the formed substrate radical (after HAT) delocalizing over the keto-group or aryl-ring. We surmise that the formed radical does not undergo radical rebound readily with Co^{III}–F and decays via alternative (non-fluorinating) pathways, meaning Co^{II} was no longer accessible (see below).

SF can itself act as an indiscriminate electrophilic fluorination reagent of certain substrates under certain conditions, without the addition of a metal catalyst.[38d,e] We therefore performed a series of control experiments involving the reaction of SF with a variety of hydrocarbons (including 1-adamantanol, cyclohexane, n-decane, methylheptanoate, toluene, and ethylbenzene) at 50 °C in CH_3CN, thus mimicking the procedure developed for the Co catalysts described above, however without the Co catalyst. We did not identify any fluorinated products in these reactions while noting that the only F-containing species in the reaction mixture was unreacted SF according to ^{19}F NMR (Figures S37–S43).

Probing the Reaction Mechanism

In conclusion, a variety of saturated hydrocarbons were fluorinated in reasonable to high yields employing Co^{II} catalysts. Once CsF was included into the catalytic mixture, near-quantitative yields of mono-fluorinated products were obtained with remarkably high levels of selectivity for 1-adamantanol and comparable functionalized derivatives. Given the high yields and apparent selectivity, we felt it important to decipher the active oxidant and fluorinating reagents in this process. We have proposed two plausible reaction mechanisms (Schemes 3, S1): in the proposed mechanisms we have included the additive CsF because it produced near quantitative 3FA (>90 %), whereas in its absence the maximum yields were ~55 %. The depicted mechanisms represent the most plausible pathways supported by a thorough analysis of the post-reaction mixture and a series of chemical probe studies and kinetic experiments as described below.

The so-called *N-radical pathway* involves SF acting as a formal F-atom ($F^{\bullet}$) donor to Co, oxidizing Co^{II} to the corresponding to Co^{III}–F alongside the generation of the N-radical species $TEDA^{\bullet+}$ (N-(chloromethyl)triethylenediaminyl radical). $TEDA^{\bullet+}$ is postulated to act as the H-atom acceptor in hydrocarbon activation yielding a carbon-centered radical and H-TEDA. The carbon-centered radical is postulated to rebound with a Co^{III}–F adduct to facilitate C–F bond formation and yield Co^{II} which can subsequently activate another molecule of SF. An alternative to the involvement of Co^{III}–F rebounding is to make analogy to the Cu-catalyzed fluorination reported by Lectka and co-workers where an autocatalytic mechanism was invoked and SF was the rebounding entity (*cascade pathway*, Scheme S1).[15a,e] In the cascade, once $TEDA^{\bullet+}$ has formed it would induce a cascade of C–H activation (by $TEDA^{\bullet+}$) and SF N–F homolysis (by the formed C-radical, yielding a C–F bond and another equivalent of $TEDA^{\bullet+}$), *with no further involvement of Co.*

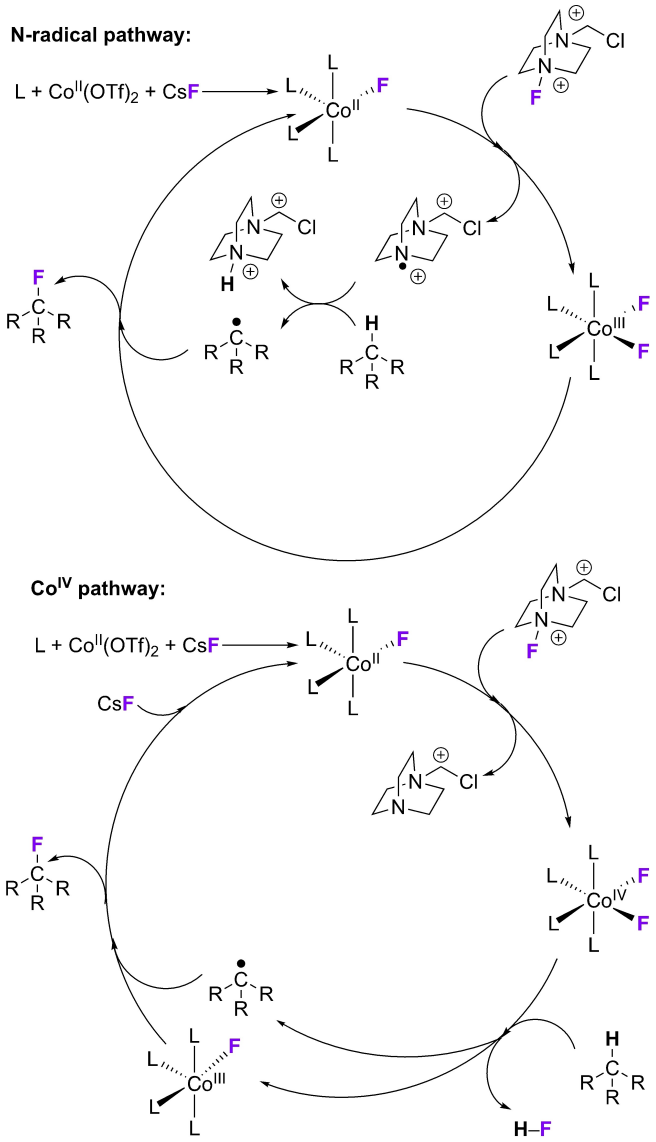

Scheme 3. Plausible mechanisms for Co^{II}-catalyzed fluorination using SF.

For the so-called *Co^{IV} pathway*, we propose that SF acts as a formal F-ion-donor (F$^+$) oxidizing **1F** to Co^{IV}–(F)$_2$ and converting SF to TEDA (which would have no further role). The Co^{IV}–(F)$_2$ would act to abstract an H-atom from the hydrocarbon yielding a carbon-centered radical, Co^{III}–F, and H–F. C–F bond formation would then be mediated by a Co^{III}–F entity yielding Co^{II} and the fluorinated hydrocarbon. In this pathway, there would be no involvement of TEDA$^{\bullet+}$, but both TEDA and H-TEDA are plausible products (depending on whether the formed H–F would protonate TEDA). Importantly, the Co^{IV} pathway allows for the formation of H–F in the reaction mixture.

Each pathway relies on the generation of an H-atom abstracting entity (TEDA$^{\bullet+}$ or Co^{IV}–(F)$_2$) and an F-atom rebounding entity (SF or Co^{III}–F), producing 3FA. Different derivatives of SF could be produced whether the N-radical (H-TEDA) or Co^{IV} pathways (TEDA and H–F) were followed, although H–F could plausibly protonate TEDA producing H-TEDA in the latter. We have explored the mechanism in detail because we believe that the involvement of a Co–F complex in the fluorination of hydrocarbons, rather than TEDA$^{\bullet+}$ and/or SF, may allow us to induce selectivity using the polyamine supporting ligands, mirroring successes achieved in the nonheme iron hydroxylation field employing analogous ligands.[13d] We have endeavored to understand the mechanism through a series of mechanistic probe experiments and kinetic analyses.

Post-Reaction Analysis

We characterized the products derived from 1-adamantanol, SF, and **1** in the post-reaction mixture in order to understand the nature of the active oxidant and fluorinating entity. Evaporation of CH_3CN from the post-catalysis reaction mixture followed by a crude ^{1}H NMR in CD_3CN showed signals only in the diamagnetic region ($\delta = 0$–10 ppm, Figures S44–S46). It should be noted that the post-reaction mixture had been exposed to air—if Co^{II} or H–F were present they were likely converted to Co^{III} and lost to the atmosphere, respectively. Apart from this, the appearance of signals in the $\delta = 7.5$–9.0 ppm region indicated the presence of arene C*H* groups, presumably from pyridine groups of the BPMEN ligand. Signals in the $\delta = 0$–5.6 ppm region were assumed to be derivatives of 1-adamantanol, SF, and the catalyst.

Isolation of 3FA: Column chromatography of the crude mixture allowed us to obtain 3FA in 56 % isolated yield from the standard conditions (see Supporting Information for details, Figures S47–S50). Crystals suitable for X-ray diffraction analysis were grown from slow evaporation of a CH_2Cl_2 solution of 3FA at room temperature. The X-ray crystallography alongside NMR, FT-IR, and ESI-MS of the isolated 3FA confirmed that the obtained 3FA displayed selective fluorination at the tertiary carbon atom in 1-adamantanol (Figure 4).

Derivatives of SF: From a standard catalysis run (Co^{II}-(OTf)$_2$/BPMEN/SF/1-adamantanol), SF was postulated to decay to yield either N-(chloromethyl)triethylenediamine chloride (TEDA) or its protonated analogue H-TEDA alongside free H–F or F$^-$. In a sealed reaction vessel, ^{19}F NMR showed the presence of free H–F ($\delta = 182$ ppm, Figure S51), appearing at the previously observed resonance in CD_3CN.[39] When CsF was employed, H–F was also observed (Figure S17). However, in the worked-up post-reaction ^{19}F NMR spectrum all H–F had been lost, presumably through evaporation. H–F is thus one of the derivatives of SF in the reaction mixture.

We independently synthesized or isolated from a post catalysis reaction mixture both TEDA and H-TEDA, respectively. Single crystals of each suitable for X-ray diffraction measurements were obtained (Figure 4, see Supporting Information file for details and spectroscopic data, Figures S44–S45, S52–S61). ^{1}H NMR and FT-IR analysis of these independently synthesized compounds allowed us to verify that H-TEDA was the SF-decay product in the

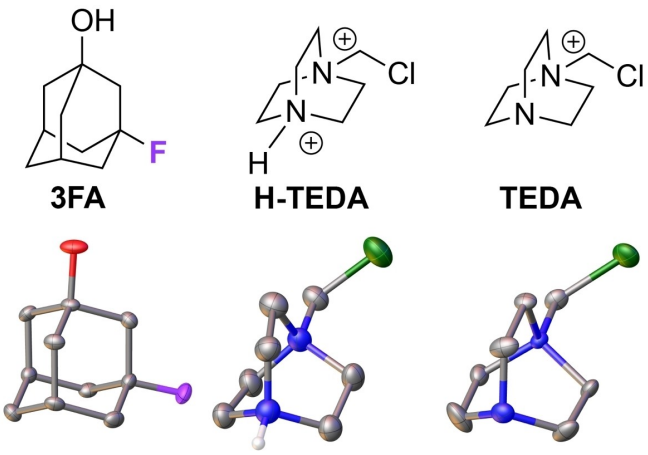

Figure 4. ORTEP of 3FA (left), H-TEDA (middle), and TEDA (right). Displacement parameters shown at 50% probability. The F atom in 3FA was disordered over three locations (see Supporting Information and commentary therein for further details). Hydrogen atoms omitted for clarity apart from N–*H* of H-TEDA.

post-reaction mixture in the absence of CsF and TEDA was the product in the presence of CsF: (i) The ^{1}H NMR of SF showed three signals at δ = 5.34, 4.78, and 4.34 ppm assigned to the three different C*H*$_2$ environments in the molecule; (ii) ^{1}H NMR of the post-reaction mixture showed signals at δ = 5.22, 3.85, and 3.75 ppm, attributed to the three C*H*$_2$ resonances, alongside a singlet at δ = 7.37 ppm that we have attributed to an N*H* (verified through the independently synthesized H-TEDA); (iii) ^{1}H NMR of a post-reaction mixture when CsF was present showed signals at lower-field at δ = 4.99, 3.43, and 3.25 ppm that we have attributed to TEDA, suggesting the deprotonated form was present when CsF was employed. (iv) The isolated H-TEDA was reacted with CsF in CD_3CN in a *J-Young* NMR tube showing an immediate shift in ^{1}H NMR resonances of H-TEDA yielding those attributed to TEDA (Figure S46). Moreover, a sharp signal at δ = −182 ppm was observed in ^{19}F NMR suggesting the formation of H–F. Thus CsF is acting as a base during the catalytic cycle, releasing H–F from H-TEDA. In conclusion, H-TEDA was obtained in a standard run and TEDA was the SF decay product in the presence of CsF.

Co-containing products: Post-reaction ESI-MS analysis only showed one mass ion that contained Co: $[Co(BPMEN)]^{2+}$ (m/Z = 164.0612, Figure S52). In the ^{1}H NMR of the post-reaction mixture were signals at δ = 6–9 ppm attributed to the Co-based products of the reaction (Figures S45): as described below, depending on the conditions used, the following three Co^{III} complexes were identified as products (Figure 3): a *bis*-nitrile complex $[Co^{III}(NCCH_3)_2(BPMEN)]^{3+}$ (**2**); a monofluoride $[Co^{III}(F)(NCCH_3)(BPMEN)]^{2+}$ (**3**); and the difluoride $[Co^{III}(F)_2(BPMEN)]^{+}$ (**4**).

We independently reacted **1** with SF (1.2 equiv.) in CH_3CN in the absence of a substrate (see Supporting Information for details). Crude analysis of the ^{1}H NMR of this reaction showed the same aromatic and aliphatic resonances were obtained as in the post-catalysis reaction mixture, albeit the intensities of the respective signals differed (Figures S44–S45). From this crude mixture, the CH_3CN was removed under vacuum and dry acetone was added to the remaining sludge yielding a red solid and acetone washings that were collected (described below). Recrystallization of the red solid from CH_3CN/Et_2O yielded the *bis*-acetonitrile complex **2** as brick red crystals. FT-IR of **2** showed a feature at $\nu_{C\equiv N} = 2327\ cm^{-1}$ (Figures S62), which we assigned to Co-bound CH_3CN ligands. Single crystal X-ray crystallography of **2** displayed a structure remarkably similar to that obtained for **1**, albeit with shorter Co^{III}-ligand bond lengths. Two $^{-}BF_4$ and one ^{-}OTf were observed in the crystal lattice and can be quantified by ^{19}F NMR (Figure S63), confirming the Co^{III} oxidation state. The Co–N_{py} (1.941(2) Å and 1.948(2) Å) and Co–N_{am} (1.968(2) Å and 1.973(2) Å) bond lengths were shorter than observed in **1** consistent with the higher oxidation state in **2** (Tables S3–S4).[27] **2** displayed the cis-α coordination geometry of BPMEN, as observed for **1**, suggesting that the BPMEN ligand maintained a strict binding environment at Co in such complexes.

^{1}H NMR of **2** showed a spectrum consistent with BPMEN ligated to a diamagnetic Co^{III} ion in a highly symmetric environment (Figures S63–S66). Of importance, ^{1}H NMR revealed a doublet that integrated for two hydrogens at δ = 8.94 ppm assigned to pyridine α–C protons, and a triplet that integrated for two hydrogens at δ = 8.36 ppm, assigned to the pyridine β–C protons. These resonances are useful for identification purposes as described below. ^{19}F NMR of **2** showed two peaks at δ = −79.0 ppm and −151.1 ppm which were assigned to the ^{-}OTf and $^{-}BF_4$ anions, respectively, confirming the crystallographic observation of both anions being present. Critically, analysis of the post-catalysis reaction ^{1}H NMR and comparison to the authentic ^{1}H NMR of **2** showed that **2** was found in the post-reaction mixture (Figures S45, S64).

Multiple recrystallizations from the acetone washings using acetone/Et_2O yielded a purple crystalline product assigned to $[Co^{III}(F)(X)(BPMEN)]^{2+}$ (X = CH_3CN or H_2O, defined as **3**). The FT-IR of **3** displayed a feature at $\nu_{C\equiv N} = 2331\ cm^{-1}$ (Figure S67), which was slightly shifted with respect to that obtained for **2** ($\nu_{C\equiv N} = 2327\ cm^{-1}$), indicating that **3** contained a metal-bound nitrile group. Furthermore, FT-IR showed a feature at $\nu_{Co-F} = 564\ cm^{-1}$ that we have assigned to a Co–F stretch based on comparable metal-fluoride complexes in the literature (note for **1F**, ν_{Co-F} was found at 571 cm^{-1}, Figure S21).[37] ESI-MS of **3** displayed a signal at m/Z = 174.0581 that can be attributed to a monofluoride $[Co(F)(BPMEN)]^{2+}$ ion (expected m/Z = 174.0575, Figure S68). ^{1}H NMR of **3** showed a total of six resonances in the aromatic region (δ = 9.1–7.5 ppm, compared to just four observed for **2**), alongside eight further features in the aliphatic region (Figures S69–S70). This is consistent with a complex that displays non-equivalent ancillary *cis*-donor ligands bonded to a Co/BPMEN core (thus F and $NCCH_3$, for example). Furthermore, seventeen signals were found in the ^{13}C NMR with the signal at δ = 5.8 ppm was assigned to a coordinated CH_3CN (Figure S71). In the ^{19}F NMR of **3**, we identified a broad signal ranging from δ = −539 to −561 ppm

that we posit is from a Co-bound F-ligand (with multiplicity consistent with a neighboring I = 7/2 ^{59}Co ion),[40] alongside a sharp signal at δ = −151.55 ppm which was attributed to $^{-}BF_4$ (Figures S72–S73). Based on the combined FT-IR, NMR, and ESI-MS data, we concluded that **3** was the mixed-ligand $[Co^{III}(F)(NCCH_3)(BPMEN)]^{2+}$.

Crystals of **3** suitable for X-ray diffraction measurements were grown from Et_2O vapor diffusion into a CH_3CN solution over three days. The crystallography showed that **3** contained a Co^{III} ion ligated by BPMEN in the same *cis*-α fashion as observed for **1**, **1F**, and **2**, while the 5th and 6th sites were occupied by ^{-}F and H_2O ligands (Figure 4, Tables S3–S4). We believe adventitious H_2O is the source of H_2O in the structure of **3**. Critically, the ^{1}H NMR of the crystals of **3** were identical to that of the isolated **3**, suggesting that the H_2O was derived from the crystallization process. The Co–N_{py} (1.93 Å) and Co–N_{am} (1.97 Å) bond lengths of **3** were shorter than those in **1** (2.12 and 2.16 Å, respectively) and almost identical to **2** (1.94 and 1.97 Å, respectively). The Co–F bond (1.868 Å) was similar to the previously reported $[Co(F)_3(Me_3TACN)]$ (1.857–1.871 Å, Me_3TACN = 1,4,7-trimethyl-1,4,7-triazacyclononane), but was shorter than **1F** (2.036 Å and 2.051 Å).[37] Analysis of the post-catalysis reaction ^{1}H NMR and comparison to the authentic ^{1}H NMR of **3** showed that **3** was found in the post-reaction mixture (Figures S45, S69). Thus, in the absence of CsF, **2** and **3** were the Co-containing products of the reaction.

When **1** was reacted with SF in the presence of CsF the *bis*-fluoride complex $[Co^{III}(F)_2(BPMEN)]^+$ (**4**) was obtained. Purple crystals of **4** suitable for X-ray diffraction measurements were grown from Et_2O vapor diffusion into an acetone solution of **4** (Tables S3–S4). Two different types of crystals were obtained which have been defined as **4**-OTf and **4**-BF_4 (ratio = 95:5). X-ray crystallographic studies of both crystals revealed a $[Co^{III}(F)_2(BPMEN)]^+$ cationic core with different counter-ions in each crystal ($^{-}$OTf and $^{-}BF_4$). We believe the source of anion mixing is that **1** contains two $^{-}$OTf anions, while SF has two $^{-}BF_4$ anions, therefore the same Co-containing cation was formed, however it could crystallize with either anion. With respect to **1**, the Co–N_{Py} and Co–N_{am} bond lengths were shorter by 0.19 Å (1.92 versus 2.11 Å in **1**). The Co–F distances in **4** were slightly shorter compared to monofluoride complex **3** (1.843 Å and 1.853 Å versus 1.8687 Å). The Co–F distances were similar but very slightly shorter than observed for $[Co(F)_3(Me_3TACN)]$ (1.857–1.871 Å),[37] and $[Fe(F)_3(TPY)]$ (1.8774–1.9062 Å, TPY = 2,2':6',2''-terpyridine).[37] In contrast, both $[Mn^{III}(F)_2(TBDAB)]^+$ (1.812 and 1.807 Å) and $[Mn^{IV}(F)_2(TBDAB)]^{2+}$ (1.7847 and 1.7840 Å, TBDAP = N,N-di-*tert*-butyl-2,11-diaza[3.3](2,6)-pyridinophane)[41] displayed shorter Mn–F bonds than $[Co^{III}(F)_2(BPMEN)]^+$. The disparities are presumably dependent on the nature of the supporting ligand as well as the inherent charge at the metal site. Importantly, as with **1**, the BPMEN ligand was ligated in a *cis-α* configuration, and the two F-ligands were thus ligated *cis* with respect to each other.

^{19}F NMR of **4** (using the combined crystals) showed two signals at δ = −78.85 ppm and −151.48 ppm corresponding to $^{-}$OTf and $^{-}BF_4$ (~5 % compared to $^{-}$OTF, Figures S74–S76), respectively. Furthermore, a very broad signal at δ = −540 to −570 ppm was identified, which was tentatively assigned to the Co^{III}-bound fluorides, again displaying multiplicity indicative of interaction with an I = 7/2 ^{59}Co ion. This signal was comparable to that observed for **3** indicating that it was likely a feature associated with Co-bound F atoms. ^{1}H NMR of **4** displayed signals consistent with a highly symmetric diamagnetic species displaying four C*H* resonances in the aromatic region, four CH_2 and one CH_3 resonance in the aliphatic region (consistent with the crystal structure, Figures S77–S79). ESI-MS analysis showed an ion at m/z = 367.1159, which was assigned to $[Co^{III}(F)_2(BPMEN)]^+$ (expected m/Z = 367.1139, Figure S80). The FT-IR of **4** displayed two signals ν_{Co-F} = 534, 554 cm^{-1} which we assign to the Co–F stretches (Figures S81–S82). A similar feature was observed for **3** (564 cm^{-1}) and **1F** (571 cm^{-1}). These values closely match those found for $[Co(F)_3(Me_3TACN)]$ (ν_{Co-F} = 574 cm^{-1}).[37] Critically, in the ^{1}H NMR analysis of the post-catalysis reaction mixture, when CsF was present, signals that can be attributed to **2**, **3**, and **4** were observed (Figures S45, S84). However, when no CsF was present, we did not observe **4**. Interestingly, the catalytic reaction mixture was blue in color when CsF was present (the color of **4** was blue) and without CsF it was pink. **4** was thus one of the Co-containing species in the reaction mixture when CsF was present.

Critically, we investigated the efficacy of the Co^{III} complexes **2** and **4** as catalysts in the oxidative fluorination of 1-adamantanol (Table 3, Figures S85–S86). Neither of the Co^{III} complexes were capable of producing 3FA in high yields (3 % and 0 %, respectively) and likewise, neither was effective at activating SF (9 % and 18 % decay, respectively). This contrasts starkly with Co^{II}, which demonstrated effective 3FA production as long as a labile ancillary ligand was present. This has led us to emphasize that the catalytic cycles postulated must cycle through Co^{II}.

In summary, analysis of the post-reaction mixture showed fluorinated organic product 3FA, free H–F, and the derivative of SF, TEDA, in both its protonated and deprotonated state (in the absence and presence of CsF, respectively). Co^{III} products **2**, **3**, and **4** (when CsF was present) were identified through independent synthesis efforts in combination with ^{1}H NMR spectroscopy and other spectroscopic techniques. The Co^{III} complexes were not effective catalysts.

Monitoring the Reaction in Real-Time

We monitored the real-time evolution of ^{1}H and ^{19}F NMR resonances during a catalysis run (Figures S87–S89).[42] As in the post-reaction mixture, ^{19}F NMR signals assigned to H-TEDA (δ = 7.38, 5.22, 3.85, 3.75 ppm) *and* H–F (δ = −182 ppm) were observed. ^{1}H NMR showed that the Co^{II} complex **1** remained present in the reaction mixture throughout a catalysis run. The observation of **1** supports our observation that the Co^{III} complexes were not catalytically active. Finally, ^{1}H NMR signals showed the mono-

fluoride **3** being dominant in the absence of CsF. A gradual appearance of **2** over time was identified (δ = 9.02 ppm), alongside depletion of **3** (δ = 8.93 ppm), indicating that as the reaction progressed and F-concentration depleted, the *bis*-acetonitrile complex **2** was favored. Thus, **1**, **2**, and **3** were the identifiable Co-containing species while both H-TEDA and H–F were derivatives of SF present during a standard catalysis run.

EPR of **1** in the solid state displayed a very broad signal centered at $g = 3.8$ at 77 K (Figure S13). EPR analysis of a catalytic reaction mixture involved generating an as-concentrated-as-possible solution (starting [**1**] = 32 mM) and analyzing the frozen solution during the reaction. This EPR spectrum showed a signal similar to the Co^{II} signal attributed to **1** (g~3.8) alongside a very weak signal centered at g = 2.00 that could be attributed to either an organic radical *or* a Co-centered radical (Figures S90, S102). The signal was quite broad, indicative of a metal-centered radical rather than an organic species. We conclude that it is plausibly associated with an $S = \frac{1}{2}$ Co^{IV} ion. Multiple attempts to improve the resolution and quality of the EPR signals failed to provide deeper insight.

ESI-MS analysis of a reaction between **1** and SF showed a mass ion at m/Z = 183.0728 which can be assigned to the Co^{IV}–$(F)_2$ species $[Co(BPMEN)+(F)_2-H]^{2+}$ (Figure S91). This ion could also be assigned as a ligand-fluorinated product $[Co^{III}+F\text{-}BPMEN+F]^{2+}$. However, in the presence of substrate this mass signal was not observed (Figure S92), suggesting that under active fluorination conditions this species was not present. Furthermore, it was not observed in any of the post reaction mixtures, nor do we have any evidence for ligand fluorination in the post-reaction mixtures. ESI-MS thus suggests that the reaction of **1** with SF may yield a Co^{IV}–$(F)_2$ species, which supports the EPR indication of a transient Co^{IV} entity.

We assessed the effect of substrate deuteration on the yields of fluorinated products in order to assess any potential kinetic isotope effect (KIE, Figures S93–S94). We performed the competitive fluorination of tetrahydrofuran (THF) and D_8-THF in the same reaction vessel (per-deuterated 1-adamanatnol was not commercially available).[42] By ^{19}F NMR we observed three new signals at δ = −111.2, −112.6, and −188.0 which were attributed to 2-fluorotetrahydrofuran (2-F-THF),[18] per-deutero-2-fluorotetrahydrofuran (2-F-D_7-THF), and 3-fluorotetrahydrofuran (3-F-THF).[43] Tatlow and co-workers showed that 2-F-THF readily rearranged to 3-F-THF.[43] Because of this, we summed the integrals to assess the total yield of fluorinated THF. The ratio of (2 + 3)-F-THF to 2-F-D_7 - THF (k_H/k_D) in the final reaction mixture was determined to be 4.7. We performed the same one-pot competition analysis on cyclohexane and its per-deuterated analogue, obtaining a KIE $k_H/k_D = 2.0$. C–H bond dissociation energies ($BDE_{C\text{-}H}$) are weaker than $BDE_{C\text{-}D}$, thus the obtained KIE values indicated that the activation of the C–H bond in THF and cyclohexane was rate-limiting in the Co-catalyzed reaction. The KIE was within the classical limit (2–7) and indicated that either proton transfer (PT) or PCET were rate-limiting. The obtained KIE values were within the range of previously reported high-valent metal-halide oxidants (M = Fe, Ni),[17a,b,d,f] but were lower than observed for M=O, which display a degree of tunneling (KIE > 20).[44] In conclusion, the KIE values demonstrated that PT or PCET from the substrate was rate-limiting.

Using D_8-THF as a model substrate we performed an Eyring analysis. We employed D_8-THF because a single product was obtained and the rate of the reaction was reasonable in the temperature window available to us (293–318 K, see Supporting Information file for details). The activation enthalpy ($\Delta H^{\ddagger}$) was determined to be 4.9 kcal mol^{-1}, while the activation entropy ($\Delta S^{\ddagger}$) was determined to be −39 cal mol^{-1} K^{-1} (Figure S95, Table S2). The large and negative value of $\Delta S^{\ddagger}$ was consistent with a bimolecular reaction and aligns with the characteristics of previously reported high-valent metal-mediated oxidation reactions (large and negative $\Delta S^{\ddagger}$).[45] In contrast, organic radical oxidants (e.g. $TEDA^{\bullet+}$) generally display small $\Delta S^{\ddagger}$ values. During HAT by an oxidant, the contribution of vibrational entropy is considerably greater for metal-mediated HAT in comparison to processes involving organic radicals. In combination with the KIE observation that indicated PT or PCET were rate-limiting, the activation parameters were consistent with a high-valent Co entity (Co^{IV}–$(F)_2$) acting as the C–H oxidant.

In summary, real-time NMR analysis indicated that Co^{II} **1** was ever-present in the reaction mixture while Co^{III}–F **3** was present in greater concentration early in the reaction and was replaced with bis-acetonitrile complex **2** as F-was incorporated into 3FA. EPR suggested the formation of a transient Co^{IV} species, which was supported by ESI-MS that indicated the involvement of a Co^{IV}–$(F)_2$ moiety in hydrocarbon fluorination. Substrate KIE values in the classical range (2–7) showed that PCET or PT was rate-limiting in 3FA formation, while an Eyring analysis confirmed the involvement of a metal ion in this rate-limiting step. In all, the real-time monitoring supported the Co^{IV} mechanism.

Radical Interception Studies

We performed the catalyzed reaction in the presence of a variety of organic radical traps (Schemes S2, S3). First, we added TEMPO (2,2,6,6-tetramethylpiperidine-1-oxyl, 5 equiv.) prior to the addition of SF in a standard catalysis experiment. In the post-reaction mixture, we observed a significantly reduced yield of 3FA (2 %, versus 56 % when no TEMPO present) despite complete consumption of SF (Table 4, Figure S96). Analysis of the post-reaction ESI-MS showed a mass peak (m/Z = 308.2611) that could be attributed to the $[TEMPO + adamantan\text{-}1\text{-}ol - H]^+$ ion (predicted mass = 308.2584, Figure S97). This product presumably formed from the coupling of a carbon-centered 1-adamantanol radical and TEMPO. This provides strong evidence for the formation of a carbon-centered radical, indicating PCET C–H activation during the reaction. Furthermore, an alternative radical trap DMPO (5,5-dimethyl-1-pyrroline-N-oxide) produced the same outcome as evidenced by ESI-MS showing a mass peak that could be

Table 4: Mechanistic catalysis studies.[a]

Catalyst	additive	SF consumed (%)	3FA yield (%)	TEDA-X yield[b]	other fluorinated yield (%)
1	TEMPO	100	2	0	–
1	DMPO	74	7	0	–
1	GD	100	7	0	67 (Ph_3CF)
–	GD	100	11	0	53 (Ph_3CF)
1	$^nBu_4NPF_6$	90	57	0	–
1	Fluorobenzene[c]	26	–	0	0
1	Toluene[c]	78	–	0	13 ($PhCH_2F$)

[a] Conditions: 10 mol% Co; SF 10 equiv.; T = 50 °C, t = 2 h. [b] X = TEMPO/DMPO/CPh_3. [c] t = 40 h.

assigned to the $[DMPO+adamantan\text{-}1\text{-}ol-H]^+$ formula (expected m/Z = 264.1964, found m/Z = 264.2172, Figures S98–S99). As with TEMPO, DMPO reduced the yield of 3FA dramatically (7%, Figure S100). Importantly, these studies did not show any evidence for TEDA/TEMPO or TEDA/DMPO coupling products forming by ESI-MS.

DMPO itself is EPR silent (unlike TEMPO), but upon reaction with an organic radical will yield an oxyl-radical that can be probed using EPR. Therefore, any radicals that are identified in the DMPO reaction mixture likely derived from an organic radical *or* are associated with the active oxidant. EPR analysis of the DMPO reaction mixture after 5 minutes showed a very low intensity signal centered at g = 2.00 that appeared to display significant hyperfine splitting (Figure S101). This signal appears similar to those obtained when DMPO reacted with carbon-centered radicals,[46] that is the DMPO-decay product radical $[DMPO+adamantan\text{-}1\text{-}ol-H]^+$ (identified above using ESI-MS). Generally such species have a short lifetime.[46d] We took another sample after 2 h and the EPR spectrum showed a different signal at g = 2.00 alongside depleted DMPO-coupling product signal. We tentatively attribute the new and more intense feature to a low spin Co^{IV} intermediate. Interestingly, this EPR signal was similar but not identical to that obtained during monitoring of the catalysis reaction mixture by EPR (centered at g = 2.00, Figure S102).[47] We believe the new g = 2.00 species accumulated because the normal decay pathways for Co^{IV} were interrupted: In the absence of substrate and DMPO, we postulate that Co^{IV} disproportionated with Co^{II} to yield two Co^{III}. In the presence of substrate, Co^{IV} reacted with substrate to produce Co^{III} and a carbon-centered radical, followed by RR to yield Co^{II}. In the presence of DMPO, Co^{II} will not form because the carbon centered radical reacted with DMPO, meaning Co^{IV} accumulates. We tentatively conclude that EPR analysis of the DMPO interception mixture demonstrates accumulation of a Co^{IV} entity.

Gomberg's dimer (GD) acts as a disguised trityl radical which can be used as a reliable test for fluorine atom transfer (FAT) reactivity.[48] GD formed trityl fluoride in just 5% yield when reacted with equimolar SF when tested under the standard reaction conditions (CH_3CN, 50 °C, Figure S103). SF was thus a poor F-atom donor to GD. Expanding on this observation, we performed a Co^{II}-catalyzed reaction in the presence of GD. In the presence of GD (10 equiv.) the yield of 3FA dropped to just 7% (*cf* 56%), while the yield of tritylfluoride was 67% and all SF was consumed (Figure S104). Thus, GD inhibited 3FA production *and* appears to act as an F-atom acceptor from a Co–F adduct in doing so. No evidence for 1-adamantanol/GD or TEDA/GD coupling products was obtained by ESI-MS of the GD inhibited reaction (Figure S106).

We explored chemical methods to prove the formation of $TEDA^{\bullet+}$ through the addition of substrates that we anticipated would intercept this N-radical cation:

(i) We anticipated that a tetraalkylamonium cation might undergo alkyl radical transfer with a transient $TEDA^{\bullet+}$. We performed a standard catalysis reaction in the presence of a tetra-n-butylammonium hexafluorophosphate ($^nBu_4NPF_6$) in the anticipation that *n*Bu-TEDA would form from a reaction between $TEDA^{\bullet+}$ and $^nBu_4N^+$ alongside inhibiting 3FA formation. ^{19}F NMR of the post reaction mixture revealed the same yield of 3FA as obtained under standard conditions (57%, Figure S107). Furthermore, we did not identify any ESI-MS signals that could be attributed to *n*Bu-TEDA (Figure S108).

(ii) Ritter and co-workers demonstrated a Pd-catalyzed N-arylation, where the newly formed N-aryl group was derived from SF. They invoked a mechanism involving a transient $TEDA^{\bullet+}$, derived from SF, coupling with a non-activated arene (Ar) to yield Ar-TEDA. Indeed, they obtained Ar-TEDA products postulated to be derived from $TEDA^{\bullet+}$.[49] Based on this, we envisioned that arenes would intercept $TEDA^{\bullet+}$ if it formed during the Co-catalyzed fluorination. We performed the Co-catalyzed fluorination in the presence of fluorobenzene and toluene in the expectation that FC_6H_4-TEDA and tolyl-TEDA, respectively, would form if $TEDA^{\bullet+}$ was present. ESI-MS and ^{19}F NMR spectroscopy of the post reaction mixture containing fluorobenzene did not indicate the formation of FC_6H_4-TEDA (Figures S109–S110). Furthermore, NMR analysis of the toluene-containing mixture, only showed evidence for fluoromethylbenzene formation (13%, Table 4), with no indications of tolyl-TEDA (Figures S111–S112).

In summary, radical trapping studies demonstrated that TEMPO, DMPO, and GD all inhibited 3FA production, indicating that they were intercepting a C-centered radical or F-atom donors, respectively, involved in oxidative fluorination. We identified the substrate/radical coupling products

TEMPO/DMPO + adamantan-1-ol showing the interception of substrate radicals while the reaction in the presence of GD showed the formation of trityl fluoride confirming the interception of F-atom donor species. Importantly, no evidence for $TEDA^{\bullet+}$-radical coupling products was obtained.

Fluorine Atom Transfer Studies

We next explored the efficacy of **3** and **4** as F-atom donor reagents (Scheme 4, Figures S113–S120). It is important to recall that SF was deemed an ineffective FAT reagent under the current reaction conditions. **3** and **4** were reacted with GD (1 equiv. CH_3CN, 25 °C) showing conversion to trityl-fluoride in 31 % and 67 % yields, respectively, according to ^{19}F NMR. In the **4** + GD post-reaction mixture, ESI-MS showed peaks at m/z = 164.5570, 364.1057, 478.0935 which can be assigned to $[Co^{II}(BPMEN)]^{2+}$, $[[Co^{II}(BPMEN)]+Cl]^{+}$, and $[[Co^{II}(BPMEN)]+OTf]^{+}$, the same ions observed for **1** and **1F**, indicating the reformation of Co^{II} upon F-atom transfer. When we carried out these reactions in an N_2-filled *J-Young* NMR tube in CD_3CN, by ^1H NMR we observed all the aromatic protons (δ = 6–9 ppm) assigned to **3** and **4** disappear and new paramagnetic signals appearing (δ = 0–220 ppm), that match well with those observed for **1** in the case of **3** and for **1F** when **4** was reacted. Thus, the diamagnetic Co^{III} complexes **3** and **4** effected FAT to GD producing tritylfluoride and Co^{II} products **1** and **1F**. This demonstrates both **3** and **4** to be F-atom donors and to be catalytically relevant—it is worth recalling that neither **3** nor **4** were effective catalysts. To probe this further, the **4** + GD post-reaction solution was subsequently charged with 1-adamantanol and SF, producing 3FA in 9 % yield under the standard catalysis conditions. Under standard catalytic conditions, GD inhibited 3FA formation (11 % yield), thus the obtained yield is consistent with the active catalyst being generated. The F-atom transfer reaction between **3** or **4** and GD thus produced a catalytically relevant entity.

Discussion of Mechanistic Analysis

Co^{II} salts catalyzed the oxidative fluorination of saturated hydrocarbons in high yields in the presence of polydentate amine donor ligands. Both poly-amine (e.g. cyclam) and mixed amine/pyridine (e.g. BPMEN) displayed catalytic efficacy. The addition of CsF enhanced these yields to close to quantitative conversion of 1-adamantanol to 3FA. Importantly, only Co^{II} facilitated the high-yield conversion, while Fe, Ni, and Cu salts did not produce notable yields. This is despite the observation that both BPMEN on its own and the $[M(BPMEN)]^{2+/+}$ (M = Fe, Ni, Cu) catalysts facilitated near-complete depletion of SF without producing notable yields of 3FA. Until now, SF activation had been postulated to produce $TEDA^{\bullet+}$ which would then facilitate fluorination via a radical cascade mechanism. In the present example, the radical cascade mechanism was not invoked, and we have demonstrated that Co must be involved.

In the post-reaction mixture, besides the fluorinated product 3FA, H-TEDA, TEDA, and H–F were identified alongside Co^{III} complexes **2**, **3**, and **4**. Real-time monitoring of the reaction mixture showed both **2** and **3** were present and that the concentration of **2** increased as the concentration of **3** decreased as the reaction progressed (as more fluoride was incorporated into 3FA). This indicated that **3** was the F-atom donor, which was supported by separate reactivity studies between **3** and GD. In the presence of CsF, real-time monitoring showed **4** in the reaction mixture and **4** was also found to be a highly effective F-atom donor. We concluded that a Co^{III}–F was the likely F-atom donor and SF was not involved in F-atom donation.

We initially proposed that $TEDA^{\bullet+}$ or Co^{IV} were the active PCET C–H oxidant and endeavored to obtain evidence for both species in the reaction mixture. No evidence for the involvement of $TEDA^{\bullet+}$ was obtained. Importantly, we identified several sets of conditions where SF was consumed (presumably producing $TEDA^{\bullet+}$) but no 3FA was obtained—this indicated that even if $TEDA^{\bullet+}$ was generated it was not responsible for oxidative fluorination. Using both ESI-MS and EPR spectroscopy, we provided indications of the involvement of a Co^{IV}–$(F)_2$ entity. Furthermore, our kinetic analyses suggested that PCET was rate-limiting and that the active oxidant employed a metal

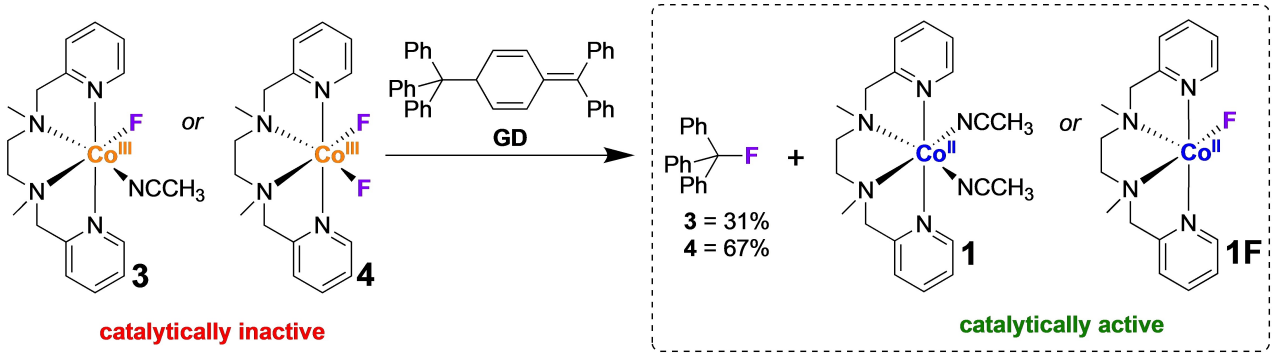

Scheme 4. Reaction of **3** and **4** with GD to produce trityl fluoride and catalytically active **1** and **1F**, respectively.

ion. We therefore conclude that the Co^{IV} pathway was the most plausible mechanism for oxidative fluorination using Co^{II} catalysts, employing Co^{IV}–$(F)_2$ for PCET C–H activation followed by RR with a Co^{III}–F moiety.

Conclusions

We have demonstrated the application of Co^{II} salts in combination with polydentate N-donor ligands for the oxidative fluorination of saturated hydrocarbons employing Selectfluor as a fluorine source. The incorporation of CsF as an additive produced near-quantitative yields of fluorinated saturated hydrocarbons. Our method thus demonstrates the activation of very strong C–H bonds in saturated hydrocarbons and the effective replacement of H-atoms with F-atoms therein. For 1-adamantane-derived substrates, we demonstrated selective fluorination at the 3-position. We have proposed two plausible reaction mechanisms: *either* (i) an N-radical, derived from Selectfluor, acted as the C–H oxidant followed by radical rebound with SF or Co^{III}–F *or* (ii) a Co^{IV}–$(F)_2$ species was responsible initially for C–H activation and the formed radical rebounded with the Co^{III}–F product to produce fluorinated hydrocarbon. Our combined evidence indicated that an N-radical was not the active oxidant *and* SF was not the rebounding entity. We concluded that a Co^{IV}–$(F)_2$ species was the likely active oxidant and Co^{III}–F was the likely F-atom donor to a carbon centered radical producing a C–F bond. Our methods take inspiration from the heme and nonheme iron family of oxygenases that employ Fe=O for C–H activation and the formed radical rebounds with Fe–OH to yield hydroxylated products. We continue to explore these catalysts for selective hydrocarbon fluorination through manipulation of the ligand framework.

Acknowledgements

This publication has emanated from research supported by Science Foundation Ireland under grant number SFI/21/FFP–P/10161 and the Irish Research Council under grant number IRCLA/2022/2957. We thank Dr. John O'Brien and Dr. Manuel Ruether for assistance with NMR. We thank Prof. Robert Barklie for training on and use of an EPR spectrometer. Open Access funding provided by IReL.

Conflict of Interest

The authors declare no conflict of interest.

Data Availability Statement

The data that support the findings of this study are available from the corresponding author upon reasonable request.

Keywords: Bioinorganic Chemistry · High-Valent Oxidant · Nonheme Iron and Cobalt · Hydrocarbon Oxidation

[1] a) B. A. Arndtsen, R. G. Bergman, T. A. Mobley, T. H. Peterson, *Acc. Chem. Res.* **1995**, *28*, 154–162; b) K. I. Goldberg, A. S. Goldman, *Acc. Chem. Res.* **2017**, *50*, 620–626.

[2] a) E. I. Solomon, D. E. Heppner, E. M. Johnston, J. W. Ginsbach, J. Cirera, M. Qayyum, M. T. Kieber-Emmons, C. H. Kjaergaard, R. G. Hadt, L. Tian, *Chem. Rev.* **2014**, *114*, 3659–3853; b) A. Migliore, N. F. Polizzi, M. J. Therien, D. N. Beratan, *Chem. Rev.* **2014**, *114*, 3381–3465; c) T. L. Poulos, *Chem. Rev.* **2014**, *114*, 3919–3962; d) C. E. Elwell, N. L. Gagnon, B. D. Neisen, D. Dhar, A. D. Spaeth, G. M. Yee, W. B. Tolman, *Chem. Rev.* **2017**, *117*, 2059–2107; e) V. C. Wang, S. Maji, P. P. Chen, H. K. Lee, S. S. Yu, S. I. Chan, *Chem. Rev.* **2017**, *117*, 8574–8621; f) X. Huang, J. T. Groves, *Chem. Rev.* **2018**, *118*, 2491–2553.

[3] a) D. P. Galonic, E. W. Barr, C. T. Walsh, J. M. Bollinger Jr., C. Krebs, *Nat. Chem. Biol.* **2007**, *3*, 113–116; b) M. L. Matthews, C. S. Neumann, L. A. Miles, T. L. Grove, S. J. Booker, C. Krebs, C. T. Walsh, J. M. Bollinger Jr., *Proc. Natl. Acad. Sci. USA* **2009**, *106*, 17723–17728; c) S. D. Wong, M. Srnec, M. L. Matthews, L. V. Liu, Y. Kwak, K. Park, C. B. Bell, 3rd, E. E. Alp, J. Zhao, Y. Yoda, S. Kitao, M. Seto, C. Krebs, J. M. Bollinger, Jr., E. I. Solomon, *Nature* **2013**, *499*, 320–323.

[4] a) L.-P. Zhao, B. K. Mai, L. Cheng, F. Gao, Y. Zhao, R. Guo, H. Wu, Y. Zhang, P. Liu, Y. Yang, *Nat. Synthesis* **2024**, *3*, 967–975; b) Q. Zhao, Z. Chen, J. Soler, X. Chen, J. Rui, N. T. Ji, Q. E. Yu, Y. Yang, M. Garcia-Borràs, X. Huang, *Nat. Synthesis* **2024**, *3*, 958–966.

[5] a) W. Liu, J. T. Groves, *Acc. Chem. Res.* **2015**, *48*, 1727–1735; b) J. P. Biswas, S. Guin, D. Maiti, *Coord. Chem. Rev.* **2020**, *408*, 213174.

[6] a) E. I. Solomon, T. C. Brunold, M. I. Davis, J. N. Kemsley, S.-K. Lee, N. Lehnert, F. Neese, A. J. Skulan, Y.-S. Yang, J. Zhou, *Chem. Rev.* **2000**, *100*, 235–350; b) P. Comba, S. Wunderlich, *Chem. Eur. J.* **2010**, *16*, 7293–7299; c) A. R. McDonald, L. Que, *Coord. Chem. Rev.* **2013**, *257*, 414–428; d) M. Puri, L. Que Jr., *Acc. Chem. Res.* **2015**, *48*, 2443–2452; e) S. Chatterjee, T. K. Paine, *Angew. Chem. Int. Ed.* **2016**, *55*, 7717–7722; f) M. Puri, A. N. Biswas, R. Fan, Y. Guo, L. Que Jr., *J. Am. Chem. Soc.* **2016**, *138*, 2484–2487; g) G. Li, A. K. Dilger, P. T. Cheng, W. R. Ewing, J. T. Groves, *Angew. Chem. Int. Ed.* **2018**, *57*, 1251–1255; h) S. Rana, J. P. Biswas, A. Sen, M. Clemancey, G. Blondin, J. M. Latour, G. Rajaraman, D. Maiti, *Chem. Sci.* **2018**, *9*, 7843–7858; i) A. J. Jasniewski, L. Que Jr., *Chem. Rev.* **2018**, *118*, 2554–2592; j) K. Bleher, P. Comba, D. Faltermeier, A. Gupta, M. Kerscher, S. Krieg, B. Martin, G. Velmurugan, S. Yang, *Chem. Eur. J.* **2022**, *28*, e202103452.

[7] a) J. Huang, C. Li, B. Wang, D. A. Sharon, W. Wu, S. Shaik, *ACS Catal.* **2016**, *6*, 2694–2704; b) M. Srnec, E. I. Solomon, *J. Am. Chem. Soc.* **2017**, *139*, 2396–2407.

[8] a) D. A. Petrone, J. Ye, M. Lautens, *Chem. Rev.* **2016**, *116*, 8003–8104; b) R. Szpera, D. F. J. Moseley, L. B. Smith, A. J. Sterling, V. Gouverneur, *Angew. Chem. Int. Ed.* **2019**, *58*, 14824–14848.

[9] a) O. Jacobson, D. O. Kiesewetter, X. Chen, *Bioconjugate Chem.* **2015**, *26*, 1–18; b) R. Halder, T. Ritter, *J. Org. Chem.* **2021**, *86*, 13873–13884.

[10] a) S. Rozen, *Acc. Chem. Res.* **1988**, *21*, 307–312; b) T. B. Patrick, S. Khazaeli, S. Nadji, K. Hering-Smith, D. Reif, *J. Org. Chem.* **1993**, *58*, 705–708.

[11] M. Schappacher, R. Weiss, R. Montielmontoya, A. Trautwein, A. Tabard, *J. Am. Chem. Soc.* **1985**, *107*, 3736–3738.

[12] a) T. Furuya, A. S. Kamlet, T. Ritter, *Nature* **2011**, *473*, 470–477; b) T. Furuya, T. Ritter, *J. Synthetic Org. Chem. Japan* **2011**, *69*, 48–61; c) M. G. Campbell, T. Ritter, *Chem. Rev.* **2015**, *115*, 612–633; d) C. Chatalova-Sazepin, R. Hemelaere, J.-F. Paquin, G. M. Sammis, *Synthesis* **2015**, *47*, 2554–2569; e) Q. Cheng, T. Ritter, *Trends Chem.* **2019**, *1*, 461–470.

[13] a) I. Garcia-Bosch, I. Prat, X. Ribas, M. Costas, Wiley-VCH Verlag GmbH & Co. KGaA, **2012**, pp. 27–46; b) W. N. Oloo, L. Que Jr., *Acc. Chem. Res.* **2015**, *48*, 2612–2621; c) X. Huang, J. T. Groves, *J. Biol. Inorg. Chem.* **2017**, *22*, 185–207; d) M. C. White, J. Zhao, *J. Am. Chem. Soc.* **2018**, *140*, 13988–14009; e) M. Milan, M. Salamone, M. Costas, M. Bietti, *Acc. Chem. Res.* **2018**, *51*, 1984–1995.

[14] a) W. Liu, J. T. Groves, *J. Am. Chem. Soc.* **2010**, *132*, 12847–12849; b) W. Liu, X. Huang, M. J. Cheng, R. J. Nielsen, W. A. Goddard, 3rd, J. T. Groves, *Science* **2012**, *337*, 1322–1325; c) J. T. Groves, W. Liu, X. Huang, WO/2013/028639A1, **2013**; d) W. Liu, J. T. Groves, *Angew. Chem. Int. Ed.* **2013**, *52*, 6024–6027; e) W. Liu, X. Huang, J. T. Groves, *Nat. Protoc.* **2013**, *8*, 2348–2354; f) X. Huang, W. Liu, H. Ren, R. Neelamegam, J. M. Hooker, J. T. Groves, *J. Am. Chem. Soc.* **2014**, *136*, 6842–6845; g) X. Huang, W. Liu, J. M. Hooker, J. T. Groves, *Angew. Chem. Int. Ed.* **2015**, *54*, 5241–5245.

[15] a) S. Bloom, C. R. Pitts, D. C. Miller, N. Haselton, M. G. Holl, E. Urheim, T. Lectka, *Angew. Chem. Int. Ed.* **2012**, *51*, 10580–10583; b) S. Bloom, C. R. Pitts, R. Woltornist, A. Griswold, M. G. Holl, T. Lectka, *Org. Lett.* **2013**, *15*, 1722–1724; c) S. Bloom, J. L. Knippel, M. G. Holl, R. Barber, T. Lectka, *Tet. Lett.* **2014**, *55*, 4576–4580; d) S. Bloom, J. L. Knippel, T. Lectka, *Chem. Sci.* **2014**, *5*, 1175–1178; e) C. R. Pitts, S. Bloom, R. Woltornist, D. J. Auvenshine, L. R. Ryzhkov, M. A. Siegler, T. Lectka, *J. Am. Chem. Soc.* **2014**, *136*, 9780–9791; f) C. R. Pitts, B. Ling, R. Woltornist, R. Liu, T. Lectka, *J. Org. Chem.* **2014**, *79*, 8895–8899; g) S. A. Harry, M. R. Xiang, E. Holt, A. Zhu, F. Ghorbani, D. Patel, T. Lectka, *Chem. Sci.* **2022**, *13*, 7007–7013.

[16] a) Y. Amaoka, M. Nagatomo, M. Inoue, *Org. Lett.* **2013**, *15*, 2160–2163; b) Y. Takahira, M. Chen, Y. Kawamata, P. Mykhailiuk, H. Nakamura, B. K. Peters, S. H. Reisberg, C. Li, L. Chen, T. Hoshikawa, T. Shibuguchi, P. S. Baran, *Synlett* **2019**, *30*, 1178–1182; c) S. Yakubov, W. J. Stockerl, X. Tian, A. Shahin, M. J. P. Mandigma, R. M. Gschwind, J. P. Barham, *Chem. Sci.* **2022**, *13*, 14041–14051.

[17] a) P. Mondal, P. Pirovano, A. Das, E. R. Farquhar, A. R. McDonald, *J. Am. Chem. Soc.* **2018**, *140*, 1834–1841; b) P. Mondal, M. Lovisari, B. Twamley, A. R. McDonald, *Angew. Chem. Int. Ed.* **2020**, *59*, 13044–13050; c) P. Mondal, A. R. McDonald, *Chem. Eur. J.* **2020**, *26*, 10083–10089; d) C. Panda, L. M. Doyle, R. Gericke, A. R. McDonald, *Angew. Chem. Int. Ed.* **2021**, *60*, 26281–26286; e) M. Lovisari, R. Gericke, B. Twamley, A. R. McDonald, *Inorg. Chem.* **2021**, *60*, 15610–15616; f) C. Panda, O. Anny-Nzekwue, L. M. Doyle, R. Gericke, A. R. McDonald, *JACS Au* **2023**, *3*, 919–928.

[18] J. K. Bower, A. D. Cypcar, B. Henriquez, S. C. E. Stieber, S. Zhang, *J. Am. Chem. Soc.* **2020**, *142*, 8514–8521.

[19] X.-G. Zhang, P. Guo, J.-F. Han, K.-Y. Ye, *Chem. Commun.* **2020**, *56*, 8512–8523.

[20] P. Guo, Y. Li, X.-G. Zhang, J.-F. Han, Y. Yu, J. Zhu, K.-Y. Ye, *Org. Lett.* **2020**, *22*, 3601–3606.

[21] a) Y.-R. Luo, *Comprehensive Handbook of Chemical Bond Energies*, CRC Press, Boca Raton, **2007**; b) X.-S. Xue, P. Ji, B. Zhou, J.-P. Cheng, *Chem. Rev.* **2017**, *117*, 8622–8648.

[22] $^{-}BF_4$ signals were integrated against the residual ^{-}OTf signals associated with the catalyst, showing no depletion of either entity.

[23] S. Min, B. Park, J. Nedsaengtip, S. Hyeok Hong, *Adv. Synth. Catal.* **2022**, *364*, 1975–1981.

[24] U. Knof, A. von Zelewsky, *Angew. Chem. Int. Ed.* **1999**, *38*, 302–322.

[25] a) C. R. Goldsmith, C. M. Coates, K. Hagan, C. A. Mitchell, *J. Mol. Catal. A* **2011**, *335*, 24–30; b) Z. Zhang, K. L. Coats, Z. Chen, T. J. Hubin, G. Yin, *Inorg. Chem.* **2014**, *53*, 11937–11947.

[26] a) D. Quiñonero, K. Morokuma, D. G. Musaev, R. Mas-Ballesté, L. Que, *J. Am. Chem. Soc.* **2005**, *127*, 6548–6549; b) A. Marti, L. Richter, C. Schneider, *Synlett* **2011**, *2011*, 2513–2516; c) C. M. Coates, K. Hagan, C. A. Mitchell, J. D. Gorden, C. R. Goldsmith, *Dalton Trans.* **2011**, *40*, 4048–4058; d) A. Thibon, V. Jollet, C. Ribal, K. Sénéchal-David, L. Billon, A. B. Sorokin, F. Banse, *Chem. Eur. J.* **2012**, *18*, 2715–2724; e) A. Trehoux, Y. Roux, R. Guillot, J.-P. Mahy, F. Avenier, *J. Mol. Catal. A* **2015**, *396*, 40–46; f) A. Bohn, K. Sénéchal-David, J. Vanoutryve, R. Guillot, E. Rivière, F. Banse, *Eur. J. Inorg. Chem.* **2017**, *2017*, 3057–3063; g) S. Resa, A. Millán, N. Fuentes, L. Crovetto, M. Luisa Marcos, L. Lezama, D. Choquesillo-Lazarte, V. Blanco, A. G. Campaña, D. J. Cárdenas, J. M. Cuerva, *Dalton Trans.* **2019**, *48*, 2179–2189; h) S. Li, H. Li, C.-H. Tung, L. Liu, *ACS Catal.* **2022**, *12*, 9143–9152.

[27] J. F. Khosrowabadi Kotyk, C. M. Hanna, R. L. Combs, J. W. Ziller, J. Y. Yang, *Chem. Sci.* **2018**, *9*, 2750–2755.

[28] a) N. Singh, J. Niklas, O. Poluektov, K. M. Van Heuvelen, A. Mukherjee, *Inorg. Chim. Acta* **2017**, *455*, 221–230; b) P. H. A. Kankanamalage, D. M. Ekanayake, N. Singh, A. C. P. de Morais, S. Mazumder, C. N. Verani, A. Mukherjee, M. Lanznaster, *New J. Chem.* **2019**, *43*, 12795–12803; c) N. K. Botcha, R. R. Gutha, S. M. Sadeghi, A. Mukherjee, *Photosynth. Res.* **2020**, *143*, 143–153.

[29] T. Pandiyan, H. J. Guadalupe, J. Cruz, S. Bernès, V. M. Ugalde-Salvdivar, I. González, *Eur. J. Inorg. Chem.* **2008**, *2008*, 3274–3285.

[30] B. Wang, L. Wang, J. Lin, C. Xia, W. Sun, *ACS Catal.* **2023**, *13*, 10386–10393.

[31] a) L. Sacconi, *J. Chem. Soc. A: Inorganic, Physical, Theoretical* **1970**, 248–256; b) L. Sacconi, *Coord. Chem. Rev.* **1972**, *8*, 351–367; c) M. Y. Combariza, R. W. Vachet, *J. Phys. Chem. A* **2004**, *108*, 1757–1763.

[32] a) W. R. Scheidt, *J. Am. Chem. Soc.* **1974**, *96*, 84–89; b) W. R. Scheidt, *J. Am. Chem. Soc.* **1974**, *96*, 90–94; c) P. N. Dwyer, P. Madura, W. R. Scheidt, *J. Am. Chem. Soc.* **1974**, *96*, 4815–4819; d) W. R. Scheidt, J. A. Ramanuja, *Inorg. Chem.* **1975**, *14*, 2643–2648; e) V. V. Smirnov, E. K. Woller, S. G. DiMagno, *Inorg. Chem.* **1998**, *37*, 4971–4978; f) K. Ishizu, J. Hirai, M. Kodama, E. Kimura, *Chem. Lett.* **2006**, *8*, 1045–1048; g) J. Li, B. C. Noll, A. G. Oliver, G. Ferraudi, A. G. Lappin, W. R. Scheidt, *Inorg. Chem.* **2010**, *49*, 2398–2406.

[33] G. Magri, A. Folli, D. M. Murphy, *Eur. J. Inorg. Chem.* **2022**, *2022*, e202101071.

[34] Y. Kutin, N. Cox, W. Lubitz, A. Schnegg, O. Rüdiger, *Catalysts* **2019**, *9*, 926.

[35] J. Thomas-Colwell, A. Sookezian, D. A. Kurtz, J. Kallick, L. M. Henling, T. A. Stich, M. G. Hill, B. M. Hunter, *Inorg. Chem.* **2022**, *61*, 12625–12634.

[36] A. R. Corcos, O. Villanueva, R. C. Walroth, S. K. Sharma, J. Bacsa, K. M. Lancaster, C. E. MacBeth, J. F. Berry, *J. Am. Chem. Soc.* **2016**, *138*, 1796–1799.

[37] P. J. Blower, W. Levason, S. K. Luthra, G. McRobbie, F. M. Monzittu, T. O. Mules, G. Reid, M. N. Subhan, *Dalton Trans.* **2019**, *48*, 6767–6776.

[38] a) S. Rozen, C. Gal, *J. Org. Chem.* **1987**, *52*, 2769–2779; b) S. Rozen, C. Gal, *J. Org. Chem.* **1988**, *53*, 2803–2807; c) G. A. Olah, X.-Y. Li, Q. Wang, G. K. Surya Prakash, *Synthesis* **1993**, *1993*, 693–699; d) R. D. Chambers, A. M. Kenwright, M. Parsons, G. Sandford, J. S. Moilliet, *J. Chem. Soc. Perkin Trans. 1* **2002**, 2190–2197; e) R. D. Chambers, M. Parsons, G.

Sandford, E. Thomas, J. Trmcic, J. S. Moilliet, *Tetrahedron* **2006**, *62*, 7162–7167.
[39] K. O. Christe, W. W. Wilson, *J. Fluorine Chem.* **1990**, *46*, 339–342.
[40] M. C. Leclerc, J. M. Bayne, G. M. Lee, S. I. Gorelsky, M. Vasiliu, I. Korobkov, D. J. Harrison, D. A. Dixon, R. T. Baker, *J. Am. Chem. Soc.* **2015**, *137*, 16064–16073.
[41] D. Jeong, Y. Lee, Y. Lee, K. Kim, J. Cho, *J. Am. Chem. Soc.* **2024**, *146*, 4172–4177.
[42] Unlike the standard catalysis experiment, this monitoring experiment was performed at 20 °C in an NMR tube because our instrumental set-up prevented accurate NMR analysis at high temperatures (>30 °C).
[43] J. Burdon, G. E. Chivers, E. F. Mooney, J. C. Tatlow, *J. Chem. Soc. C: Organic* **1969**, 1739–1746.
[44] a) Z. Z. Pan, J. H. Horner, M. Newcomb, *J. Am. Chem. Soc.* **2008**, *130*, 7776–7777; b) D. Mandal, R. Ramanan, D. Usharani, D. Janardanan, B. Wang, S. Shaik, *J. Am. Chem. Soc.* **2015**, *137*, 722–733; c) D. Mandal, S. Shaik, *J. Am. Chem. Soc.* **2016**, *138*, 2094–2097.
[45] a) E. A. Mader, E. R. Davidson, J. M. Mayer, *J. Am. Chem. Soc.* **2007**, *129*, 5153–5166; b) E. A. Mader, V. W. Manner, T. F. Markle, A. Wu, J. A. Franz, J. M. Mayer, *J. Am. Chem. Soc.* **2009**, *131*, 4335–4345.
[46] a) E. G. Janzen, J. I. P. Liu, *J. Mag. Reson. (1969)* **1973**, *9*, 510–512; b) L. D. Haire, P. H. Krygsman, E. G. Janzen, U. M. Oehler, *J. Org. Chem.* **1988**, *53*, 4535–4542; c) E. G. Janzen, Y.-K. Zhang, D. L. Haire, *Magn. Reson. Chem.* **1994**, *32*, 711–720; d) H. Taniguchi, K. P. Madden, *Radiat. Res.* **2000**, *153*, 447–453.
[47] a) B. S. Brunschwig, M. H. Chou, C. Creutz, P. Ghosh, N. Sutin, *J. Am. Chem. Soc.* **1983**, *105*, 4832–4833; b) F. C. Anson, T. J. Collins, R. J. Coots, S. L. Gipson, T. G. Richmond, *J. Am. Chem. Soc.* **1984**, *106*, 5037–5038; c) G. B. Carpenter, G. S. Clark, A. L. Rieger, P. H. Rieger, D. A. Sweigart, *J. Chem. Soc. Dalton Trans.* **1994**, 2903–2910; d) B. Ramdhanie, J. Telser, A. Caneschi, L. N. Zakharov, A. L. Rheingold, D. P. Goldberg, *J. Am. Chem. Soc.* **2004**, *126*, 2515–2525; e) E. M. Zolnhofer, M. Käß, M. M. Khusniyarov, F. W. Heinemann, L. Maron, M. van Gastel, E. Bill, K. Meyer, *J. Am. Chem. Soc.* **2014**, *136*, 15072–15078; f) S. Hong, F. F. Pfaff, E. Kwon, Y. Wang, M.-S. Seo, E. Bill, K. Ray, W. Nam, *Angew. Chem. Int. Ed.* **2014**, *53*, 10403–10407; g) Y. Liu, T.-C. Lau, *J. Am. Chem. Soc.* **2019**, *141*, 3755–3766; h) W. Mao, D. Fehn, F. W. Heinemann, A. Scheurer, D. Munz, K. Meyer, *Angew. Chem. Int. Ed.* **2021**, *60*, 16480–16486; i) J. Yang, H. T. Dong, M. S. Seo, V. A. Larson, Y.-M. Lee, J. Shearer, N. Lehnert, W. Nam, *J. Am. Chem. Soc.* **2021**, *143*, 16943–16959; j) C. V. Wilson, D. Kim, A. Sharma, R. X. Hooper, R. Poli, B. M. Hoffman, P. L. Holland, *J. Am. Chem. Soc.* **2022**, *144*, 10361–10367; k) M. Kayne, P. S. Murphy, Y. M. Kwon, Y. Lee, T. A. Jackson, D. Wang, *Chem. Eur. J.* **2024**, *30*, e202401218.
[48] a) M. Gomberg, *J. Am. Chem. Soc.* **1900**, *22*, 757–771; b) E. S. Jang, C. L. McMullin, M. Käß, K. Meyer, T. R. Cundari, T. H. Warren, *J. Am. Chem. Soc.* **2014**, *136*, 10930–10940.
[49] G. B. Boursalian, W. S. Ham, A. R. Mazzotti, T. Ritter, *Nat. Chem.* **2016**, *8*, 810–815.

Manuscript received: October 31, 2024
Accepted manuscript online: December 17, 2024
Version of record online: January 10, 2025